CLINICAL ELECTRON-BEAM DOSIMETRY

NOTE: The version published here had an incorrect value for C3 (0.01025) on page 85 equation number 13. This was corrected effective June 13th 2007. The version published in Medical Physics is correct (0.0025).

Published for the
American Association of Physicists in Medicine
by the American institute of Physics

AAPM REPORT NO. 32

CLINICAL ELECTRON-BEAM DOSIMETRY[†]

REPORT OF
TASK GROUP NO. 25
RADIATION THERAPY COMMITTEE*

AAPM

Members

Faiz M. Khan (Task Group Chairman)
Karen P. Doppke
Kenneth R. Hogstrom
Gerald J. Kutcher
Ravinder Nath
Satish C. Prasad
James A. Purdy
Martin Rozenfeld
Barry L. Werner

[†]Reprinted from MEDICAL PHYSICS, Volume 18, Issue 1, 1991

*Ravinder Nath, Radiation Therapy Committee Chairman

February 1991

Published for the
American Association of Physicists in Medicine
by the American Institute of Physics

Further copies of this report ($10 prepaid) may be obtained from:

American Institute of Physics
c/o AIDC
64 Depot Road
Colchester, Vermont 05446

(1-800-445-6638)

Library of Congress Catalog Card Number: 91-70875
International Standard Book Number: 0-88318-905-4
International Standard Serial Number: 0271-7344

Published by the American Institute of Physics, Inc.
335 East 45th Street, New York, NY 10017-3483

Printed in the United States of America

Clinical electron-beam dosimetry: Report of AAPM Radiation Therapy Committee Task Group No. 25

Faiz M. Khan, Karen P. Doppke, Kenneth R. Hogstrom, Gerald J. Kutcher, Ravinder Nath, Satish C. Prasad, James A. Purdy, Martin Rozenfeld, and Barry L. Werner
AAPM Task Group No. 25

(Received 7 May 1990; accepted for publication 24 October 1990)

TABLE OF CONTENTS

I. INTRODUCTION

High-energy electrons were first used in radiation therapy shortly after the successful extraction of the beam from a betatron in 1947. By the early 1950s a few institutions using commercial betatrons or unique linear accelerators were treating patients on a routine basis. This modality remained confined to a few major centers until the 1970s when, with the commercial development of linear accelerators with suitable energy and retractable x-ray targets, many other institutions began using electrons for radiation therapy. The basic physics and dosimetry of high-energy electrons had been established for their initial clinical use. With their increasing use, details of their clinical dosimetry, which had lagged somewhat behind the corresponding developments for high-energy x rays, have been much further developed. Over the years several symposia have been devoted to dosimetry and treatment planning with high-energy electrons. In addition, extensive literature on various aspects of the use of electrons in therapy has appeared. The International Commission on Radiation Units and Measurements (ICRU) has published an exhaustive and detailed report (ICRU, 1984) on essentially all aspects of electron-beam dosimetry, including updated values of basic dosimetry data such as stopping powers and scattering powers. That document is an excellent reference for detailed study of electron-beam dosimetry, but is not as practical for clinical use.

This monograph has been prepared by Task Group 25 of the Radiation Therapy Committee of the American Association of Physicists in Medicine (AAPM) primarily to fill the needs of a hospital physicist in the utilization of clinical electron beams of 5-25 MeV. Its scope has been restricted to (i) dosimetry measurement techniques and procedures for acquiring the basic information that is necessary for treatment planning and the acceptance testing of a new electron accelerator and (ii) the utilization of dosimetry data for the determination of monitor units. Principles of collimation and

 0094.2405/91/010073-37$01.20

their influence on the patient dose are discussed for both external and internal collimation, and the report states in an elementary manner the effect of tissue inhomogeneities on the dose distribution. Each section includes the procedure recommended by the task group for the performance measurements and calculations, the reasons for that choice, and a supporting bibliography. Implementation of the procedures recommended in this report might lead to changes in data used for treatment planning or dose calculations. If such changes would lead to significant changes in the radiotherapist's perception of treatment techniques he is familiar with, such changes must be discussed and understood before they are implemented clinically.

The scientific understanding and methodology of clinical dosimetry is still incomplete. This report intends to reflect the current side of scientific understanding and technical methodology in clinical electron dosimetry. As such it is not final, but it is offered as an up-to-date aid to the clinical physicist charged with supporting clinical electron-beam therapy. Other tasks, such as acceptance testing and commissioning of a new machine, the development of a quality assurance program and methodology for consistent treatment delivery, are separate subjects.

II. DOSE MEASUREMENT

Clinical applications of electrons for radiation therapy require that the dose in the entire irradiated volume be determinable. Similar to the procedures for radiation therapy with x rays, the dose at any point in a patient for a given number of monitor units is obtained through the following steps.

(i) Measurement of dose at a reference point (typically at the depth-of-dose maximum on the central axis) in a reference phantom (typically water) with a flat surface perpendicular to the electron-beam direction and for a reference field configuration (AAPM, 1983).

(ii) Measurement of dose at the reference point (typically at the depth of dose maximum) on central axis for the field of interest in a reference phantom relative to the dose determined in a (a) above.

(iii) Measurement of dose distributions in a reference phantom with the flat surface perpendicular to the electron beam direction, including central-axis depth-dose curves, lateral beam profiles, and isodose curves for all cones or selected field sizes of clinical interest.

(iv) Determination of dose distribution in the irradiated patient at points of interest in the tumor volume, healthy organs, and tissues at risk. Doses are obtained from calculations using the measured reference data and *in vivo* measurements of dose at points where practical.

This section describes dosimetry systems and phantoms that measure relative doses referred to in (ii), (iii), and (iv) for high-energy electron beams (5-25 MeV).

A. ionization chambers

The most commonly used dosimeters for calibration of photon and electron beams are exposure-calibrated ionization chambers. Procedures involved in the use of ionization chambers have been described in detail by the ICRU (1984)) Hospital Physicists Association (HPA, 1985), Nordic Association of Clinical Physicists (NACP, 1981) and AAPM (1983). The AAPM dosimetry protocol represents the current AAPM recommendations, and this task group recommends its adoption for calibration of electron beams. The AAPM protocol recommends that plane-parallel chambers having collection-volume heights and diameters not exceeding 2 mm and 2.0 cm, respectively, should be employed for dose calibration of electron beams with energies less than 10 MeV and either plane-parallel or cylindrical chambers for higher energy electrons. This report outlines a protocol for the measurement of dose relative to the calibration dose and hence supplements the AAPM 1983 protocol.

One disadvantage of ionization chambers for electron-beam dosimetry is that the ionization-to-dose conversion factors, such as stopping-power ratios and perturbation factors, depend strongly upon electron energy and depth in the phantom. Despite these difficulties, ionization chambers are the most commonly used instruments for measurement of dose. They are readily available, portable, and easy to use; and measurements performed with them are highly reproducible. Through their calibration by both national and international standard laboratories, they also provide an excellent means of consistency among radiation therapy centers.

In addition to low leakage current, the ionization chamber should have negligible stem and cable effects. Irradiation of the chamber's stem, collecting electrode, or cable by high-energy electrons can lead to emission of secondary electrons or collection of electrons that could produce a spurious ionization current. Stem effects should be checked carefully using a long rectangular field at two perpendicular collimator orientations, one including the stem and cable and the other excluding them. Another method for checking for these effects is by shielding the stem and cable. It should be noted that stem and cable effects depend upon electron energy, depth, and field size, and therefore should be checked at various energies and fields of interest.

Under certain conditions, the chamber polarity effect can be significant (Mattsson et al., 1981; Gerbi and Khan, 1987). To account for this effect, the ionization charge should be measured at both positive and negative polarities of the collecting electrode. The true ionization charge is given by (Pruitt, 1987),

$$Q = \frac{(Q_+ - Q_-)}{2}. \tag{1}$$

It should be noted that Q_+ and Q_- are quantities that have opposite signs except when the signal is smaller than the polarity-independent background. Averaging the absolute magnitudes of Q_+ and Q_- would result in the same value of Q as Eq. (1) except in the rare case when both Q_+ and Q_- have the same sign because of low signal-to-background ratio. By this procedure, the spurious currents arising from stem, cable, or other effects that do not change sign upon switching of polarity can be eliminated, while the component of spurious currents which changes sign with change in polarity of the bias voltage is not. The magnitude of the

polarity effect should be determined throughout the depth-dose curve for the measurement conditions.

Both cylindrical and plane-parallel ionization chambers have been used for determining central-axis depth-dose curves for electron beams. For thin plane-parallel chambers, it is generally accepted that the effective point of measurement is the front surface of the collecting volume. For a cylindrical chamber the effective point of measurement is displaced towards the source from the center of the chamber. The magnitude of this displacement has been measured by using thin plane-parallel chambers, film dosimeters, or Fricke dosimeters in thin vessels and by using a series of cylindrical probes of decreasing radii. Task Group 25, in agreement with the ICRU (1984) recommends the use of a single value of one-half the radius r of the sensitive volume for the upstream shift of effective point of measurement at all depths for all energies of clinical interest, i.e.,

$$d = d_{\text{center}} - 0.5\, r \text{ (cylindrical chambers)}, \quad (2)$$

$$d = d_{\text{front surface of collection volume}} \text{ (plane-parallelchambers)}. \quad (3)$$

(Note: The recommendation of this task group for the 0.5 r shift in depth for the cylindrical chamber is different from the 0.75 r shift of TG21.)

The following procedure is recommended for determining relative depth-dose values in a homogeneous phantom using an ionization chamber.

(i) Leakage: Check the ionization chamber for leakage. Leakage should be less than 0.1% of maximum signal.

(ii) Stability: The sensitivity of the chamber should be measured periodically. Variation in sensitivity should not be greater than 1%.

(iii) Data collection: Irradiate the chamber in a phantom (water is preferred) at the standard nominal source-to-surface distance (SSD) for treatment and measure the ionization charge as a function of depth Q(d). Charge should be collected for a set number of monitor units. Allow sufficient time for the phantom to come to equilibrium with room temperature. Measure the temperature and pressure before and after the irradiation measurements to evaluate the variation of chamber sensitivity during the course of the measurements.

(iv) Polarity: During the course of data collection, check the measured ionization readings for polarity effect by taking at least three readings each for positive and negative voltage. If polarity effects greater than 1% are found, correct all readings for polarity effect using Eq. (1). As a minimum, check the polarity effect near the surface, at depth of maximum ionization, at depth of 50% ionization, and 2 cm beyond the practical range.

(v) Ion recombination: The measured ionization readings should be corrected for ion recombination effects as described in the 1983 AAPM protocol. The ion collection efficiency correction factor P_{ion} can be obtained from Fig. 1 for voltage ratio of two (AAPM protocol, 1983) or Table I for a voltage ratio of five.

(vi) Incorporate the above corrections of polarity and ion recombination to determine the corrected ionization charge Q_{corr}.

(vii) Depth correction: For cylindrical chambers apply the upstream shift correction of one-half the radius to determine the effective point of measurement, as described earlier. Make a plot of Q_{corr}. versus the corrected depth d.

(viii) From the plot of Q_{corr}. versus d, obtain the depth of 50% ionization R_{50} and practical range R_p, and then determine the mean incident energy E_o and mean energy E_d, as a function of depth d, as described later in this report (see Sec. III) :

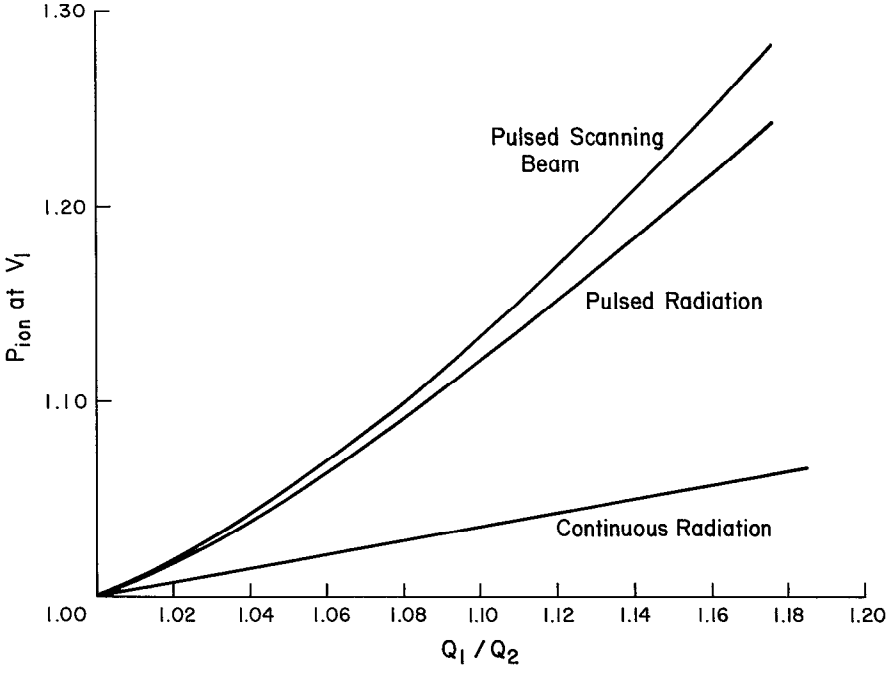

FIG. 1. Ionization recombination correction factors (P_{ion} for continuous radiation) (^{60}Co, Van de Graaf), pulsed radiation (accelerator-produced x-rays and electron beams broadened by scattering foils), and pulsed scanning beams (magnetically scanned electron beams). These data are only applicable when $V_1 = 2V_2$.

TABLE I. P_{ion} values for a voltage ratio of 5.0 (Weinhous and Meli 1984).

Voltage ratio = 5.0			
Pulsed radiation		Pulsed-swept radiation	
Charge ratio	P_{ion}	Charge ratio	P_{ion}
1.00	1.000	1.00	1.000
1.025	1.006	1.05	1.013
1.05	1.013	1.10	1.028
1.075	1.020	1.15	1.045
1.10	1.027	1.20	1.063
		1.25	1.083
1.15	1.041		
1.20	1.057	1.35	1.130
		1.45	1.186
1.30	1.091	1.55	1.254
1.40	1.130	1.65	1.335
1.50	1.174		

$$\bar{E}_d = \bar{E}_0(1 - d/R_p). \quad (4)$$

(ix) Determine the mean restricted mass collision stopping power ratio, $(\bar{L}/\rho)^{med}_{air}$, for the mean incident electron beam energy at each corrected depth of measurement from Tables II, III, or IV (reproduced from AAPM protocol, 1983).

(x) Determine the chamber replacement factor P_{repl}. For parallel-plate chambers assume unity; for cylindrical chambers, determine from Table V the value at each depth of measurement using Eq. (4) to determine the mean electron energy at depth (reproduced from AAPM protocol, 1983).

(xi) The dose to the medium is given by

$$D_{med} = Q_{corr} P_{repl} (\bar{L}/\rho)^{med}_{air} K, \quad (5)$$

where K is a depth-independent constant which equals the cavity-gas calibration factor, N_{gas} (AAPM protocol, 1983), if the charge is also corrected to 22°C and one standard atmosphere. The central-axis percent depth dose *(%D)* is given by

$$\%D(d) = 100 \frac{D_{med}(d)}{D_{med}(d_{max})}, \quad (6)$$

where d_{max} is the depth of dose maximum.

Modifications of these equations for off-axis profile measurements and output factor measurements are discussed in Secs. VI and VII, respectively.

TABLE II. Ratio of water to air mean restricted ($\Delta = 10$ keV) collision mass stopping powers, $(L/\rho)^{water}_{air}$ tabulated as a function of depth for various incident electron beam energies (AAPM, 1983).

Depth	Electron beam energy (MeV)																			
g/cm^2	60.0	50.0	40.0	30.0	25.0	20.0	18.0	16.0	14.0	12.0	10.0	9.0	8.0	7.0	6.0	5.0	4.0	3.0	2.0	1.0
0.0	0.902	0.904	0.912	0.928	0.940	0.955	0.961	0.969	0.977	0.986	0.997	1.003	1.011	1.019	1.029	1.040	1.059	1.078	1.097	1.116
0.1	0.902	0.905	0.913	0.929	0.941	0.955	0.962	0.969	0.978	0.987	0.998	1.005	1.012	1.020	1.030	1.042	1.061	1.081	1.101	1.124
0.2	0.903	0.906	0.914	0.930	0.942	0.956	0.963	0.970	0.978	0.988	0.999	1.006	1.013	1.022	1.032	1.044	1.064	1.084	1.106	1.131
0.3	0.904	0.907	0.915	0.931	0.943	0.957	0.964	0.971	0.979	0.989	1.000	1.007	1.015	1.024	1.034	1.046	1.067	1.089	1.112	1.135
0.4	0.904	0.908	0.916	0.932	0.944	0.958	0.965	0.972	0.980	0.990	1.002	1.009	1.017	1.026	1.036	1.050	1.071	1.093	1.117	1.136
0.5	0.905	0.909	0.917	0.933	0.945	0.959	0.966	0.973	0.982	0.991	1.003	1.010	1.019	1.028	1.039	1.054	1.076	1.098	1.122	
0.6	0.906	0.909	0.918	0.934	0.946	0.960	0.967	0.974	0.983	0.993	1.005	1.012	1.021	1.031	1.043	1.058	1.080	1.103	1.126	
0.8	0.907	0.911	0.920	0.936	0.948	0.962	0.969	0.976	0.985	0.996	1.009	1.016	1.026	1.037	1.050	1.067	1.090	1.113	1.133	
1.0	0.908	0.913	0.922	0.938	0.950	0.964	0.971	0.979	0.988	0.999	1.013	1.021	1.031	1.043	1.058	1.076	1.099	1.121		
1.2	0.909	0.914	0.924	0.940	0.952	0.966	0.973	0.981	0.991	1.002	1.017	1.026	1.037	1.050	1.066	1.085	1.108	1.129		
1.4	0.910	0.916	0.925	0.942	0.954	0.968	0.976	0.984	0.994	1.006	1.022	1.032	1.044	1.058	1.075	1.095	1.117	1.133		
1.6	0.912	0.917	0.927	0.944	0.956	0.971	0.978	0.987	0.997	1.010	1.027	1.038	1.050	1.066	1.084	1.104	1.124			
1.8	0.913	0.918	0.929	0.945	0.957	0.973	0.981	0.990	1.001	1.014	1.032	1.044	1.057	1.074	1.093	1.112	1.130			
2.0	0.914	0.920	0.930	0.947	0.959	0.975	0.983	0.993	1.004	1.018	1.038	1.050	1.065	1.082	1.101	1.120	1.133			
2.5	0.917	0.923	0.934	0.952	0.964	0.981	0.990	1.000	1.013	1.030	1.053	1.067	1.083	1.102	1.120	1.131				
3.0	0.919	0.926	0.938	0.956	0.969	0.987	0.997	1.008	1.023	1.042	1.069	1.084	1.102	1.119	1.129					
3.5	0.922	0.929	0.941	0.960	0.974	0.994	1.004	1.017	1.034	1.056	1.085	1.102	1.118	1.128						
4.0	0.924	0.932	0.944	0.964	0.979	1.001	1.012	1.027	1.046	1.071	1.101	1.116	1.126							
4.5	0.927	0.935	0.948	0.969	0.985	1.008	1.021	1.037	1.059	1.086	1.115	1.125	1.127							
5.0	0.929	0.938	0.951	0.973	0.990	1.016	1.030	1.049	1.072	1.101	1.123	1.126								
5.5	0.931	0.940	0.954	0.978	0.996	1.024	1.040	1.061	1.086	1.113	1.125									
6.0	0.934	0.943	0.958	0.983	1.002	1.033	1.051	1.074	1.100	1.121										
7.0	0.938	0.948	0.965	0.993	1.017	1.054	1.075	1.099	1.118	1.122										
8.0	0.943	0.954	0.972	1.005	1.032	1.076	1.098	1.116	1.120											
9.0	0.947	0.960	0.981	1.018	1.049	1.098	1.114	1.118												
10.0	0.952	0.966	0.990	1.032	1.068	1.112	1.116													
12.0	0.962	0.980	1.009	1.062	1.103															
14.0	0.973	0.996	1.031	1.095	1.107															
16.0	0.986	1.013	1.056	1.103																
18.0	1.000	1.031	1.080																	
20.0	1.016	1.051	1.094																	
22.0	1.032	1.070																		
24.0	1.048	1.082																		
26.0	1.062	1.085																		
28.0	1.071																			
30.0	1.075																			

TABLE III. Ratio of polystyrene to air mean restricted ($\Delta = 10$ keV) collision mass stopping powers, $(L/\rho)^{poly}_{air}$ tabulated as a function of depth for various incident electron beam energies (AAPM, 1983).

Depth	Electron beam energy (MeV)																			
g/cm^2	60.0	50.0	40.0	30.0	25.0	20.0	18.0	16.0	14.0	12.0	10.0	9.0	8.0	7.0	6.0	5.0	4.0	3.0	2.0	1.0
0.0	0.875	0.878	0.887	0.903	0.915	0.929	0.936	0.943	0.950	0.959	0.970	0.975	0.982	0.990	0.999	1.010	1.030	1.049	1.069	1.089
0.1	0.876	0.879	0.888	0.904	0.916	0.930	0.936	0.943	0.951	0.960	0.970	0.977	0.983	0.991	1.000	1.011	1.032	1.052	1.074	1.100
0.2	0.876	0.880	0.889	0.905	0.917	0.931	0.937	0.944	0.952	0.961	0.972	0.978	0.985	0.993	1.002	1.013	1.034	1.056	1.080	1.109
0.3	0.877	0.881	0.890	0.906	0.917	0.931	0.938	0.945	0.953	0.962	0.973	0.979	0.986	0.994	1.004	1.016	1.038	1.061	1.086	1.114
0.4	0.878	0.882	0.891	0.907	0.918	0.932	0.939	0.946	0.954	0.963	0.974	0.980	0.988	0.996	1.007	1.019	1.042	1.066	1.092	1.116
0.5	0.878	0.883	0.892	0.908	0.919	0.933	0.940	0.947	0.955	0.964	0.975	0.982	0.990	0.999	1.009	1.023	1.046	1.071	1.098	
0.6	0.879	0.883	0.893	0.909	0.920	0.934	0.941	0.948	0.956	0.965	0.977	0.984	0.992	1.001	1.012	1.027	1.051	1.076	1.103	
0.8	0.881	0.885	0.894	0.911	0.922	0.936	0.943	0.950	0.959	0.968	0.980	0.983	0.996	1.006	1.019	1.035	1.060	1.087	1.111	
1.0	0.882	0.887	0.896	0.912	0.924	0.938	0.945	0.952	0.961	0.971	0.984	0.992	1.001	1.012	1.026	1.044	1.070	1.096		
1.2	0.883	0.888	0.898	0.914	0.926	0.940	0.947	0.955	0.963	0.974	0.988	0.996	1.006	1.019	1.034	1.054	1.080	1.105		
1.4	0.884	0.889	0.900	0.916	0.927	0.942	0.949	0.957	0.966	0.978	0.992	1.001	1.012	1.026	1.043	1.064	1.089	1.111		
1.6	0.886	0.891	0.901	0.918	0.929	0.944	0.951	0.959	0.969	0.981	0.997	1.007	1.019	1.033	1.052	1.073	1.098			
1.8	0.887	0.892	0.903	0.919	0.931	0.946	0.954	0.962	0.972	0.985	1.002	1.012	1.025	1.041	1.060	1.083	1.106			
2.0	0.888	0.894	0.904	0.921	0.933	0.948	0.956	0.965	0.975	0.989	1.007	1.018	1.032	1.049	1.069	1.092	1.110			
2.5	0.891	0.897	0.908	0.925	0.937	0.954	0.962	0.972	0.984	0.999	1.020	1.034	1.050	1.070	1.091	1.108				
3.0	0.893	0.900	0.911	0.929	0.942	0.959	0.969	0.979	0.992	1.010	1.035	1.051	1.069	1.090	1.105					
3.5	0.896	0.903	0.914	0.933	0.947	0.965	0.975	0.987	1.002	1.023	1.051	1.069	1.088	1.103						
4.0	0.898	0.905	0.917	0.937	0.951	0.971	0.982	0.995	1.013	1.036	1.068	1.086	1.101							
4.5	0.900	0.908	0.920	0.941	0.956	0.978	0.990	1.005	1.024	1.051	1.085	1.099	1.105							
5.0	0.902	0.910	0.923	0.945	0.961	0.985	0.998	1.015	1.037	1.067	1.097	1.103								
5.5	0.904	0.913	0.927	0.949	0.966	0.992	1.008	1.026	1.051	1.081	1.102									
6.0	0.906	0.915	0.930	0.954	0.972	1.000	1.017	1.038	1.065	1.093										
7.0	0.910	0.920	0.936	0.963	0.984	1.018	1.040	1.063	1.089	1.100										
8.0	0.914	0.925	0.943	0.973	0.998	1.039	1.063	1.086	1.098											
9.0	0.918	0.930	0.950	0.985	1.013	1.061	1.084	1.095												
10.0	0.922	0.936	0.958	0.997	1.030	1.081	1.093													
12.0	0.931	0.949	0.976	1.024	1.067															
14.0	0.942	0.963	0.995	1.056	1.085															
16.0	0.953	0.978	1.016	1.078																
18.0	0.966	0.994	1.041																	
20.0	0.979	1.011	1.061																	
22.0	0.994	1.030																		
24.0	1.008	1.047																		
26.0	1.023	1.057																		
28.0	1.036																			
30.0	1.045																			

B. Thermoluminescent dosimeters

The principles of thermoluminescent dosimetry have been described extensively in the literature. A recent review of the use of thermoluminescent dosimeters (TLDs) for electron dosimetry by the ICRU (1984) and relatively recent textbooks on practical aspects of TLDs (Oberhofer and Scharmann, 1981; Horowitz, 1984) are excellent references for further details. High sensitivity of thermoluminescent dosimetry permits the construction of small dosimeters that can be used for measurements in regions of sharp gradients and for ***in vivo*** dosimetry. The dosimeters are sturdy and applicable to various shapes and sizes. Of the many thermoluminescent phosphors available, LiF (e.g., used in Harshaw TLD-100) is the most extensively employed. Its useful dose range for clinical electron beams extends from 10^{-5} to 10^{1} Gy and it is. highly independent of dose rate (up to 10^{9} Gy s^{-1}).

TLDs should be calibrated in a reference radiation field at the depth-of-maximum dose on or near the central axis. The TLD response per unit dose to the medium in the absence of the phosphor is defined as TLD sensitivity Sand is independent of electron energy (ICRU, 1984). There are conflicting data regarding the energy dependence of TLD sensitivity for electron beams relative to cobalt-60 gamma rays. Some investigators have observed a 10% decrease in sensitivity while others have observed no decrease (Suntharalingam and Cameron, 1969; Gantchew and Toushlekova, 1976; Shiragai, 1977). It has been speculated that this difference may arise from effects that depend upon electron energy, phosphor size and shape, and atomic composition. It is, therefore, recommended that TLDs not be calibrated using photon beams but using electron beams of energy similar to the one for intended use.

LiF dosimeters are available in the form of powder, chips, and rods. Commercially available, disposable capsules of LiF powder are frequently employed. For irradiation, the powder is usually packaged in polyethylene capsules or thin polyethylene bags that are sealed. A device that vibrates the powder and then dispenses a preassigned volume of the powder onto the planchette may be employed. For better accuracy, the mass of LiF powder should be measured using an analytical balance. The powder should be uniformly distrib-

TABLE IV. Ratio of acrylic to air mean restricted ($\Delta = 10$ keV) collision mass stopping powers, $(L/\rho)^{\text{acrylic}}_{\text{air}}$ tabulated as a function of depth for various electron beam energies (AAPM, 1983).

Depth	Electron beam energy (MeV)																			
g/cm^2	60.0	50.0	40.0	30.0	25.0	20.0	18.0	16.0	14.0	12.0	10.0	9.0	8.0	7.0	6.0	5.0	4.0	3.0	2.0	1.0
0.0	0.870	0.874	0.882	0.898	0.909	0.923	0.929	0.936	0.944	0.953	0.963	0.969	0.975	0.983	0.992	1.003	1.023	1.043	1.063	1.083
0.1	0.871	0.875	0.883	0.899	0.910	0.924	0.930	0.937	0.945	0.953	0.964	0.970	0.976	0.984	0.993	1.005	1.025	1.046	1.068	1.093
0.2	0.872	0.875	0.884	0.900	0.911	0.925	0.931	0.938	0.945	0.954	0.965	0.971	0.978	0.986	0.995	1.007	1.028	1.050	1.073	1.101
0.3	0.872	0.876	0.885	0.901	0.912	0.925	0.932	0.939	0.946	0.955	0.966	0.972	0.979	0.988	0.997	1.010	1.031	1.054	1.079	1.106
0.4	0.873	0.877	0.886	0.902	0.913	0.926	0.933	0.939	0.947	0.956	0.967	0.974	0.981	0.990	1.000	1.013	1.035	1.059	1.085	1.107
0.5	0.874	0.878	0.887	0.902	0.914	0.927	0.933	0.940	0.948	0.958	0.969	0.975	0.983	0.992	1.003	1.016	1.040	1.064	1.091	
0.6	0.875	0.879	0.888	0.903	0.915	0.928	0.934	0.941	0.949	0.959	0.970	0.977	0.985	0.994	1.006	1.020	1.044	1.069	1.095	
0.8	0.876	0.880	0.889	0.905	0.916	0.930	0.936	0.944	0.952	0.962	0.974	0.981	0.989	1.000	1.012	1.029	1.054	1.080	1.103	
1.0	0.877	0.882	0.891	0.907	0.918	0.932	0.938	0.946	0.954	0.964	0.977	0.985	0.994	1.006	1.020	1.038	1.064	1.089		
1.2	0.878	0.883	0.893	0.909	0.920	0.934	0.940	0.948	0.957	0.968	0.981	0.990	1.000	1.012	1.028	1.048	1.073	1.097		
1.4	0.880	0.885	0.894	0.910	0.922	0.936	0.943	0.951	0.960	0.971	0.986	0.995	1.006	1.020	1.037	1.057	1.083	1.103		
1.6	0.881	0.886	0.896	0.912	0.924	0.938	0.945	0.953	0.963	0.975	0.990	1.000	1.012	1.027	1.045	1.067	1.091			
1.8	0.882	0.887	0.897	0.914	0.926	0.940	0.947	0.956	0.966	0.978	0.995	1.006	1.019	1.035	1.054	1.076	1.098			
2.0	0.883	0.889	0.899	0.915	0.927	0.942	0.950	0.958	0.969	0.982	1.000	1.012	1.026	1.043	1.063	1.085	1.103			
2.5	0.886	0.892	0.902	0.919	0.932	0.948	0.956	0.965	0.977	0.992	1.014	1.028	1.044	1.063	1.085	1.101				
3.0	0.888	0.895	0.906	0.923	0.937	0.953	0.962	0.973	0.986	1.004	1.029	1.045	1.063	1.083	1.098					
3.5	0.891	0.898	0.909	0.927	0.941	0.959	0.968	0.980	0.996	1.016	1.045	1.063	1.082	1.096						
4.0	0.893	0.900	0.912	0.931	0.946	0.965	0.975	0.989	1.006	1.030	1.062	1.080	1.094							
4.5	0.895	0.903	0.915	0.935	0.951	0.971	0.983	0.998	1.018	1.045	1.079	1.092	1.097							
5.0	0.897	0.905	0.918	0.939	0.956	0.978	0.991	1.008	1.031	1.061	1.090	1.096								
5.5	0.900	0.908	0.921	0.943	0.962	0.986	1.000	1.020	1.045	1.075	1.095									
6.0	0.902	0.910	0.924	0.947	0.968	0.994	1.010	1.032	1.059	1.086										
7.0	0.905	0.915	0.930	0.957	0.981	1.012	1.033	1.058	1.083	1.092										
8.0	0.909	0.920	0.937	0.967	0.995	1.003	1.056	1.080	1.090											
9.0	0.913	0.925	0.945	0.979	1.011	1.055	1.077	1.088												
10.0	0.917	0.931	0.953	0.991	1.029	1.075	1.086													
12.0	0.926	0.943	0.970	1.018	1.067															
14.0	0.937	0.957	0.989	1.051	1.076															
16.0	0.948	0.973	1.011	1.071																
18.0	0.961	0.989	1.036																	
20.0	0.974	1.006	1.055																	
22.0	0.989	1.025																		
24.0	1.004	1.042																		
26.0	1.019	1.050																		
28.0	1.031																			
30.0	1.039																			

uted over the planchette so that it does not clump in one location.

The solid forms of LiF, i.e., chips or rods, are easier to handle than powder but require careful attention to each chip. The chips and rods must be assigned an identity number, which can be accomplished by storing them in a tray with a numbered grid of shallow holes, each holding one chip. Ideally, the tray should be made of inert material such as glass or porcelain but this can be very expensive. A less expensive method employs an aluminum tray that has been aged by about five cycles of heating to a temperature of 400°C for 8 h and cooling to room temperature. The same tray can then be used for annealing purposes. The heating cycles are necessary as a freshly machined aluminum surface is chemically reactive and will drift impurities into the TLD chips. The dosimeters can be placed in a PMMA (polymethylmethacrylate) tray with shallow holes and irradiated uniformly by a large field. From this procedure a relative factor for the sensitivity of each dosimeter can be determined by taking the ratio of the individual TLD response to the average response for the whole batch. Another option is to select TLDs that have sensitivities within a specified range (e.g., ±3%).

Chips and rods are suitable for skin dose measurements if their thickness is less than 1 mm. LiF powder, packaged in thin cellophane or similar plastic sheets, can be spread to very thin layers and also used for such measurements. Plastic capsules containing LiF powder are thicker and less de-

TABLE V. Chamber replacement factor P_{repl} for cylindrical chambers (AAPM 83).

$\bar{E}_d$	Inner diameter (mm)			
(MeV)	3	5	6	7
2	0.977	0.962	0.956	0.949
3	0.978	0.966	0.959	0.952
5	0.982	0.971	0.965	0.960
7	0.986	0.977	0.972	0.967
10	0.990	0.985	0.981	0.978
15	0.995	0.992	0.991	0.990
20	0.997	0.996	0.995	0.995

sirable due to perturbation effects and their averaging dose over their thickness.

The most commonly used annealing, irradiation and readout sequence for LiF is to anneal at 400 °C for 1 h and at 80 °C for 24 h before irradiation and to wait at least 24 h after the irradiation before the readout. However, this procedure is lengthy and alternative annealing cycles have been successfully employed. One of them requires annealing at 400 °C for 1 h followed by 100 °C for 2 h prior to irradiation; after irradiation annealing at 100 °C for 10 min is required prior to readout. The postirradiation annealing eliminates the relatively short-lived, low temperature glow peaks. No matter what thermal cycle is selected, it is important that all TLD dosimetry for electron dose measurements and calibrations undergo the identical anneal and read cycle (and that this same technique be employed from day to day). The sensitivity of the dosimeter batch must be calibrated after each annealing.

Background for TLD measurements can be measured by reading a control TLD that has not been irradiated. This measurement includes the phototube dark current, which can be estimated separately by reading the TLD analyzer without a dosimeter. A log of background readings and dark current readings is useful as part of the quality assurance program for the TLD system.

The thermoluminescent signal of LiF after irradiation fades by approximately 5% in 3 months. Care must be taken to account for this fading. One simple procedure is to measure the thermoluminescent output after a specified time (such as 24 h) for all measurements including the TLD calibration.

The dose-response curve for all TLD phosphors is linear only over a limited dose range. For LiF, the TLD response increases linearly with dose up to a value of about 200 cGy and then increases with dose by a power greater than unity (supralinearity), as shown in Fig. 2. For this reason, the calibration should be performed in approximately the same dose range as that intended for use. Otherwise, a linearity correction should be applied:

$$\text{Dose} = (\text{TL} - \text{TL}_{\text{background}})\, f_{\text{linearity}}\, S_{\text{cal}}, \qquad (7)$$

where S_{cal} is the TLD sensitivity at the calibration dose (typically 2 Gy) and $f_{\text{linearity}}$ is the ratio, (S/S_{cal}) of the sensitivity at the level of TL readout to that for the calibration condition.

With proper care, a thermoluminescence dosimetry system can be used effectively for ***in vivo*** dosimetry and measurements at specified points in phantoms simulating complex patient setups. However, thermoluminescence dosimetry cannot be conveniently used to measure the entire dose distribution in a phantom.

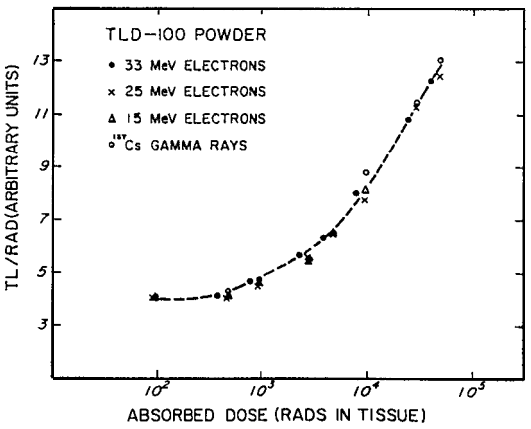

FIG. 2. Thermoluminescence sensitivity as a function of exposure (dose to tissue) for LiF TLD-100. Supralinearity of the response is shown by the departure from a constant value. (After Suntharalingam and Cameron, 1969).

C. Silicon diode dosimetry

For details of the physics of semiconductor devices, see textbooks such as the one by Sze, 1969 and Rikner's Ph.D. dissertation, 1983. Silicon diodes are small, with sensitivity thousands of times that of an air ionization chamber. These characteristics plus an instantaneous electronic response make them ideally suited for scanning devices. A typical value of radiation sensitivity in a diode with external dimensions of 2.5 X 2.5 X 0.4 mm^3 (sensitive volume of 0.3 mm^3) is 220 nC/Gy. This large signal makes the electrometer design much simpler than that required for ionization chambers.

Silicon diodes can be used directly, without depth-dependent corrections, for relative measurements of dose distributions for electron beams, provided their accuracy has been verified by comparison with ionization chamber measurements of depth dose. Since the dose rate dependence of diodes can change with time due to radiation damage, this check must be made periodically. A number of investigators have shown that, when properly used, diode measurements for electron beam central-axis depth dose can reproduce the corrected ionization chamber measurement, the agreement being better for depths greater than the depth of dose maximum (Rikner, 1983; Wong, 1987; Ten Haken et al., 1987). Good agreement is in part due to the ratio of the stopping power of silicon to that of water being essentially constant for electron energies 5-25 MeV. For shallow depths, diode measurements typically underestimate the dose by a few percent (Shortt, 1986).,

Commercial diodes can exhibit a directional dependence; the response is about 10% lower when the direction of the radiation beam is along the axis of the diode (perpendicular to the p-n junction). Since it is difficult to determine the orientation of the sensitive volume inside the diode, care must be taken to position the diode in a reproducible orientation. High-energy electrons, photons, and neutrons can displace atoms in the crystal lattice, creating imperfections that serve as traps. This radiation-induced damage reduces the sensitivity of the diode. It has been further shown that radiation damage can lead to dose-rate dependence and that these effects are considerably smaller in ***p-n*** diodes from ***p***-type silicon compared to that from n-type silicon (Rikner and Grusell, 1983) and also in Au-doped or Pt-doped n-type Si diodes (Dixon and Ekstrand, 1986). Dose-rate dependence may lead to systematic errors, which may depend upon

80

the shape of the accelerator pulse. Since the effective point of measurement, i.e., the exact location of the sensitive volume within the diode, is usually not known, the depth-dose measurements by the diode should be forced to agree with those by an ionization chamber. It has been shown that specially fabricated diodes with a well-defined measuring point near their surface can accurately measure a dose at depths as small as 1 mm (Rikner, 1985; Shortt ***et al.,*** 1986).

Since all of these effects can lead to errors in dose measurements, it is strongly advised that, before accepting the dose distribution measured by a diode, a comparison be made with a central-axis, depth-dose curve measured by an ionization chamber.

D. Film dosimetry

Film dosimetry has been used extensively as a convenient and rapid means of measuring dose distributions of therapeutic electron beams. This method has been described in detail (Dutreix and Dutreix, 1969; Hettinger and Svensson, 1967; ICRU, 1984). Film is especially important for the dosimetry of scanning electron beams where automated dosimetry system using diode or ion chambers cannot be easily employed. Film also has the property of high spatial resolution and can provide a permanent record of dose distributions.

In general, net optical density (optical density minus background fog) of an exposed film depends nonlinearly upon dose:

$$\text{Dose} = F(\text{OD})\,\text{OD}_{\text{net}}. \tag{8}$$

A plot of optical density as a function of dose to the medium in the absence of the film is called the sensitometric curve. Its shape depends on the film emulsion and development process and is known to vary from batch to batch even for the same brand of film. Therefore, published sensitometric curves should not be used for dose measurements, and a sensitometric curve for each new batch of film to be used must be determined by measurement.

If possible, film with a linear sensitometric curve should be employed. Commonly employed films for this purpose are the Kodak XV-2 (formerly labeled RP/V-2), Kodak XTL (formerly labeled RP/M) and Kodak Industrex M films. These films are linear for doses up to 50, 10, and 20 cGy, respectively. Sensitometric curves for these films are shown in Figs. 3 (a), 3 (b), and 3 (c). For the linear portion, optical density corrected for bas fog, can be used for relative dose measurement directly without any other corrections.

Fog density determined on the edge of the film far from the irradiated field can overestimate fog due to leakage radiation. For measurements in regions of low optical density, this procedure produces larger error. For better accuracy in fog subtraction, it is recommended that an unirradiated film from the same batch be processed at the same time.

Scanning electron beams must be "on" for long enough time to produce a uniform pattern (usually about one-half minute); therefore, the less sensitive films such as the Kodak XV-2 are the best choice. However, it has been shown by Ertan ***et al.*** (1984) that the Therac 20 scanning pattern almost repeats itself after five cycles (8s). Therefore, for low

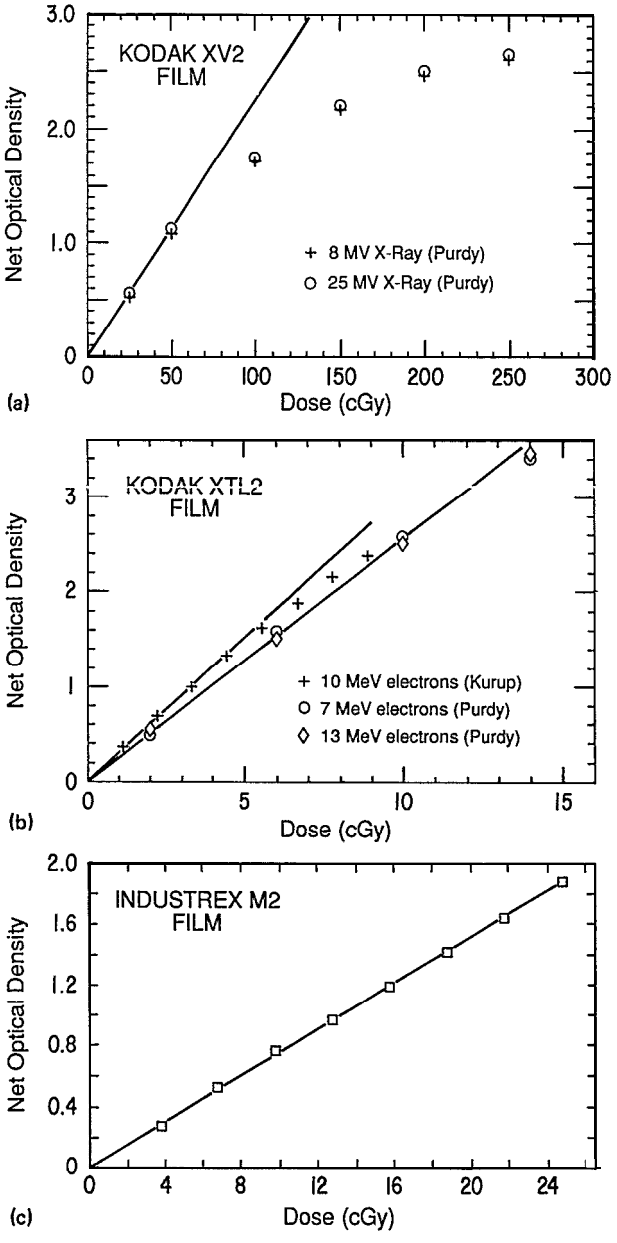

FIG. 3. (a) Sensitometric curve for Kodak XV-2 film, (b) curve for Kodak XTL film, (c) curve for Kodak Industrex M film (Shiu and Hogstrom, 1990).

dose rate (200 MU/min), it is possible to obtain data with the more sensitive films. Film is dose-rate independent for the range of dose rates found in radiotherapy, even for the pulsed-swept electron beams that have the highest dose per pulse (ICRU, 1984).

The stopping power and linear energy transfer (LET) of electrons in film emulsion begins to increase more rapidly than those of the phantom as the electron energy drops below 0.2 MeV. Despite this variation, film sensitivity has been found to be independent of electron energy and depth, making film a suitable dosimeter for measurements of central-axis depth dose for electron beams.

Film can be either perpendicular or parallel to the electron-beam axis. Under correct conditions, it has been shown

that the two geometries give the same results (Dutreix and Dutreix, 1969). For measurements with film parallel to the beam axis, precautions must be taken to align the film edge properly in the phantom slabs because film edge sticking out or pushed in produces significant distortion of the dose at shallow depths (Dutreix and Dutreix, 1969). Examples are shown in Fig. 4. For similar reasons, the film must be compressed well enough between the slabs to extrude all air. Effects of air gaps are shown in Fig. 5.

Either prepackaged film or bare film can be employed successfully provided certain precautions are followed. Prepackaged film tends to trap air in the envelope, which can be extruded by making pin pricks before compressing the film in the phantom. The film itself can move a few millimeters inside the envelope, and this motion can introduce positioning errors if not corrected. For edge-on exposure, it is necessary to fold the edge of the envelope tightly close to the film, place the envelope in the phantom, and tape the folds on the surface of the phantom. More precise positioning can be achieved by using specially designed cassettes that position the bare film in a precision-machined shallow hole such as the one shown in Fig. 6 (Bova, 1990). In order to shield out Cerenkov radiation, these cassettes made of solid water, high-impact (opaque) polystyrene, and PMMA are commercially available.

Excellent agreement with ion chamber measurement can be obtained as shown in Fig. 7 (Bova, 1990). A number of other investigators have recently reported similarly good agreement (Wong, 1987; Ten Haken et al., 1987).

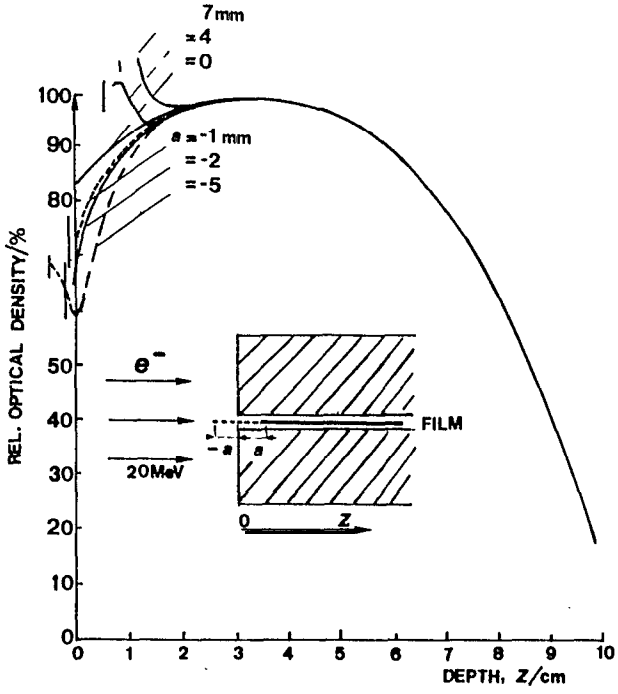

FIG. 4. Influence on the depth-density curve of maladjustment of the film edge to the phantom surface. (Dutreix and Dutreix, 1969).

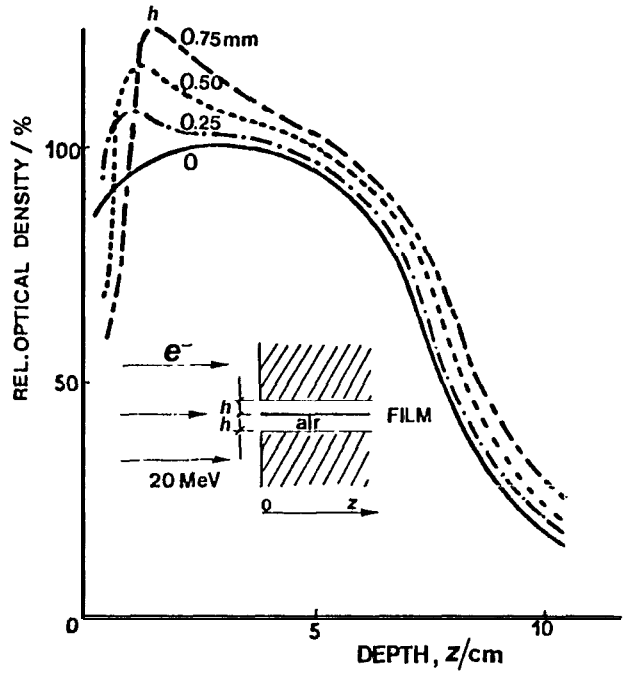

FIG. 5. Influence on the depth-density curve of thin air gaps along the film surface. Air gaps are produced on both sides of the film by strips of paper thickness h. Significant modifications of the depth-density curve are noticed even for very thin air gaps. (Dutreix and Dutreix, 1969).

E. Phantoms

It is the recommendation of this task group that water be used as the standard phantom material for dosimetry of high-energy electrons. Water is near tissue-equivalent and readily available in high purity. A water phantom tank, when empty during transportation, is also much lighter than a solid phantom. The size of the phantom must be large enough so that there is 5 cm of phantom material beyond each side of the radiation field and beyond the practical range of the electron beam. Generally, a 40-cm cube is sufficient for clinical electron beams.

1. Nonwater phantoms

It is not always possible or practical to perform dosimetry measurements in a water phantom. For example, if one is using film or an ion chamber without a waterproof sheath, then it becomes necessary to use a solid phantom. It is also difficult to make measurements near the surface of the water because of surface tension effects and the finite size of the detector.

Ideally, any solid phantom material should be water equivalent, which requires that it has the same linear collision stopping power and the same linear angular scattering power as water. This requirement can be met only if the phantom material has the same electron density and effective atomic number as water. The more popular nonwater phantoms are made of plastic, but because of their high carbon content, their effective atomic number is usually lower than that of water. This results in too low a linear angular scattering power when the linear collision stopping power

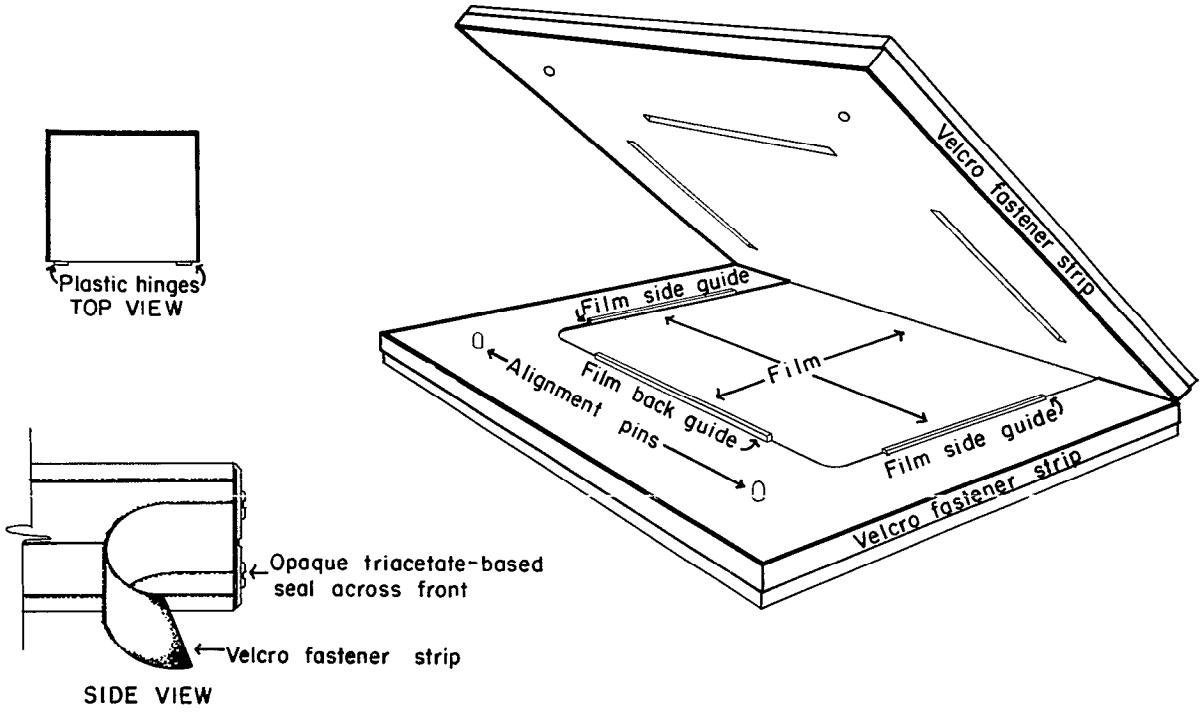

FIG. 6. Film phantom cassette. (Bova, 1990).

equals that of water. The addition of a high Z material to the plastic can reduce this difference, which is why high-impact polystyrene and "electron solid water" are often considered the most waterlike phantom materials for electron dosimetry. In nonconducting phantoms, e.g., PMMA, one must be aware of the problems resulting from charge storage (Galbraith ***et al.,*** 1984), although its effect on relative dose measurements has not been studied to date. In Table VI physical properties of solid phantom material which may be encountered in electron dosimetry are compared to those of water.

If the phantom is not water equivalent, then it will be necessary to correct the measured dose distribution for the effects of the phantom. Ideally, both the depth-dose and off-axis dose distributions should be corrected. The depth dose can be corrected (i) by properly scaling the depth in the phantom to its water-equivalent depth and (ii) by applying fluence correction factors for converting the ionization measured in the phantom to that in water. These corrections are described in the next three sections. It is the recommendation of this task group that the depth in the phantom be scaled to its water-equivalent depth for the determination of depth dose; however, the correction for differences in fluence is considered optional in a clinical environment.

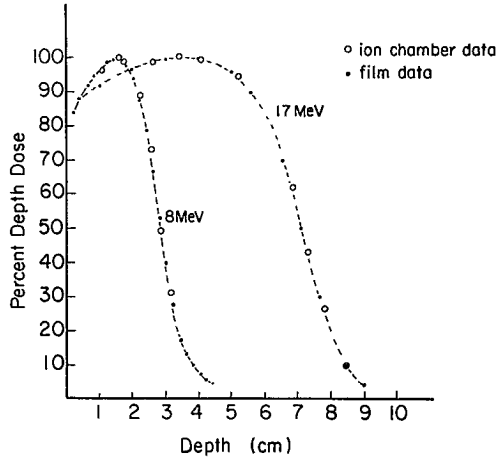

FIG. 7. Comparison of film dosimetry results with ionization chamber results. (Bova, 1990).

The corrections for the off-axis ratios are complex and have not been thoroughly investigated. It is expected that the penumbral regions of off-axis profiles are affected by the use of plastic phantoms. The penumbral shape depends on the air gap between the cone and surface and the initial angular spread of the electron beam as it passes through the collimator (Hogstrom ***et al.,*** 1981; Werner ***et al.,*** 1982) and on multiple Coulomb scatter in the phantom (Hogstrom ***et al.,*** 1981). The former effect dominates for low energy (< 10 MeV) and for large air gaps. Differences in penumbra are expected to be greatest for high energies (> 15 MeV) and depths near and beyond R_{80} (Wong, 1987). This task group recommends to take off-center ratios or profiles measured in water as the reference. At any depth, corrections for change of energy with depth should be essentially constant across the beam. Therefore, cross beam profiles measured in water, and normalized at the central ray, need no corrections. It is strongly recommended to compare, at the energy of interest, off-center profiles measured in a particular nonwater phantom, for at least one field size with the corresponding profiles

TABLE VI. Physical properties of nonwater phantoms.

Composition	Water H_2O	Clear polystyrene $(C_8H_8)_n$	High-impact polystyrene (White) $(C_8H_8)_n + TiO_2$[a]	Electron solid water [c,d]	PMMA $(C_5H_8O_2)_n$
Mass density (g cm $^{-3}$)	1.0	1.045	1.054	1.00	1.18
Electron density relative to water	1.0	1.012	1.018	1.00	1.147
Linear collision stopping power[b] at 10 MeV (MeV/cm)	1.968	2.00	2.01	1.969	2.251
Linear angular scattering power[b] at 10 MeV (radian^2/cm)	0.0695	0.0572	0.0603	0.0708	0.0713

[a] 3% TiO_2, may vary with manufacturer.
[b] Calculated from ICRU 35 (1984) unless stated otherwise.
'Ho et al., 1985; Constantinou, 1990.
'Available from Radiation Measurements, Inc., Middleton, Wisconsin.

measured in water, before using that nonwater phantom for other field sizes.

a. Conversion of dose. Dose in water at a depth d_{water} is related to the dose in the solid at a corresponding depth d_{med}, provided secondary electron equilibrium exists (normally within a few millimeters of the surface) and energy spectra at each position are identical (Brahme and Lax, 1983), by

$$D_{water}(d_{water}) = D_{med}(d_{med})\left[(\bar{S}/\rho)_{coll}\right]_{med}^{water}[\phi]_{med}^{water}, \quad (9)$$

where $\left[(\bar{S}/\rho)_{coll}\right]_{med}^{water}$ is the ratio of the mean unrestricted mass collision stopping power in water to that in the solid. $[\phi]_{med}^{water}$ is the fluence factor, that is, the ratio of the electron fluence in water to that in the solid phantom. Because energy-loss straggling and multiple scattering depend upon the effective atomic number of the phantoms, it is not possible to find corresponding depths where the energy spectra are identical. However, there are corresponding depths where the mean energies are identical. Equation (10) is assumed to hold for these depths, which are defined to be at equivalent depths.

b. Water-equivalent depth. The relationship between depth in the nonwater phantom and water-equivalent depth is a nonlinear function of depth. Near the surface as well as near the end of the practical range (R,), the depth in the nonwater phantom can be converted to water-equivalent depth by scaling it by the ratio of electron density in the nonwater phantom to that in water. This type of relationship has been used to scale the practical range in a nonwater material to that in water to be used for determining the most probably energy (NACP, 1980). However, for the measurement of depth dose in plastic phantoms, this relation results in overpredicting the penetration of the depth-dose curve near the therapeutic range (defined in Sec. V), as it neglects the effect the lower effective atomic number has on depth dose.

In an effort to estimate accurately the electron depth-dose curve near the therapeutic range and along its descending portion, this task group recommends that the water-equivalent depth be approximated using a density determined from the ratio of R_{50} penetrations by

$$d_{water} = d_{med} \times \rho_{eff} = d_{med}\left(\frac{R_{50}^{water}}{R_{50}^{med}}\right), \quad (10)$$

i.e., the effective density, r_{eff} given by the ratio of the R_{50} in water to that in the nonwater material (Hogstrom and Almond, 1982). Recommended values for r_{eff} for various solid phantoms are listed in Table VII.

The effective densities listed in Table VII taken from the literature, are based exclusively on R_{50} measurements. Systematic errors in determining the depth of the effective point of measurement of the detector in water phantoms could result in large errors in the determination of the effective density for low-energy electron beams. However, errors in the effective density are only clinically significant at the higher energies. Therefore, values for effective electron densities have been taken for 18 MeV, in cases where energy dependence has been reported. Based on the quality of the available data, it is recommended to use the tabulated r_{eff} only to the nearest 0.005. It should be noted that the density of these plastics may vary with manufacturer and batch of plastic (Schulz and Nath, 1979). The committee recommends that the mass density of each solid phantom be measured, and that the data in Table VII be corrected for each phantom accordingly.

c. Primary electron fluence correction. The fluence factor [see Eq. (9)] accounts for the difference in electron fluence at equal water-equivalent depths. This difference arises from the difference in root-mean-square angular distribution of the electrons at depth, which in turn is caused by the difference in linear scattering powers between the two media with

TABLE VII. Recommended effective density of scaling depth from nonwater phantoms to water phantoms for electron beams.

Material	Mass density (g cm^{-3})	Measured effective density	Recommended effective density
Water	1.00	···	1.00
Clear polystyrene	1.045	···	0.975
	1.04 (Loevinger *et al.*, 1961)	0.965	
	1.05 (Goede, 1985)	0.976	
	1.045 (TenHaken and Fraass, 1987)	0.986[3]	
	1.047 (Wong, 1987)	0.971[a]	
High-impact polystyrene (white)	1.055	···	0.99
	1.054 (Wong, 1987)	0.991[3]	
Electron solid water	1.04 (Ho *et al.*, 1985; Constantinou, 1990)	1.000	1.00
PMMA	1.18	···	1.115
	1.18 (Loevinger *et al.*, 1961)	1.11	
	1.18 (Goede, 1985)	1.12	

* 18 MeV data.

nearly equal electron densities. Strictly, as the equivalent depths are at different distances from the virtual source (see Sec. VIII A), the fluence factor contains also an inverse-square correction. Table VIII provides recommended values for the fluence factor as a function of depth and energy for clear polystyrene, high-impact polystyrene, and PMMA (Hogstrom and Almond, 1982). The fluence factors for electron solid water (2), being within 0.2% of unity for all energies and depths, are taken to be unity. Their theoretical calculation employs assumptions that overestimate angulation in the descending portion of the depth-dose curve; the Fermi-Eyges theory of multiple Coulomb scattering predicts a monotonically increasing value in the angular spread of the electrons on the central axis, whereas the angular spread begins to plateau just beyond the depth of R_{80} for a field size of 15 x 15 cm^2 or greater (Werner ***et al.,*** 1982 and Lax ***et al.,*** 1983). Therefore, it is recommended that the fluence ratio at R_{80} be used on the remaining, descending portion of the curve. These calculations are based on monoenergetic incident beams; it is recommended that the most probable incident energy be used for selecting the proper data from these tables. These recommendations are supported by results reported by several groups. Meyer ***et al.*** (1984) demonstrated applicability of the recommended method for measurements made in polystyrene in the buildup region of the depth-dose curve: Berkley and Hanson (1982) demonstrated its applicability for clear polystyrene and PMMA for the entire depth-dose curve. Thwaites (1985) and Bruinvis ***et al.*** (1985) reported on the calculations of dose at the depth of maximum dose.

2. Ion chamber in phantoms for measurement of depth dose

In order for Eq. (9) to apply, secondary electron equilibrium must hold, which requires that the detector be of minimal mass or be made of material identical to the phantom. Therefore, it is recommended that thick-walled ion chambers (> 0.1 g/cm^2) be irradiated in phantoms made of the same material. For example, the Memorial Holt parallel-plate chamber should be used in clear polystyrene and the PTW Markus parallel-plate chamber in PMMA. Thin-walled ion chambers, e.g., the graphite-walled Farmer chamber, can be used in any of the solid phantoms.

In the measurement of depth dose, the conversion of ionization to dose is given by Andreo ***et al.*** (1984).

$$D_{\text{water}}(d_{\text{water}}) = N_{\text{gas}} Q_{\text{corr}}(d_{\text{med}}) \left[(\bar{L}/\rho)_{\text{coll}}\right]_{\text{air}}^{\text{med}} P_{\text{repl}} \times \left[(\bar{S}/\rho)_{\text{coll}}\right]_{\text{med}}^{\text{water}} [\phi]_{\text{med}}^{\text{water}}, \quad (11)$$

where $Q_{\text{corr}}(d_{\text{med}})$ is the corrected ionization reading discussed in Sec. II A; $\left[(\bar{L}/\rho)_{\text{coll}}\right]_{\text{air}}^{\text{water}}$ is the ratio of the mean restricted mass collision stopping power in water to that in air. Percent depth dose is then given by

$$\%D_{\text{water}}(d_{\text{water}}) = \left(\frac{\{Q_{\text{corr}}(d_{\text{med}}) \times (\bar{L}/\rho)_{\text{air}}^{\text{water}} \times [\phi]_{\text{med}}^{\text{water}} \times P_{\text{repl}}\}}{[\ldots]_{\max}}\right) \times 100, \quad (12)$$

where the denominator equals the value of the numerator at the depth-of-maximum dose. Values for $\left[(\bar{L}/\rho)_{\text{coll}}\right]_{\text{air}}^{\text{med}}$ are found in Tables II-IV.

3. Film in phantoms

Film in plastic phantoms is frequently useful for the measurement of isodose curves in a plane parallel to the central axis, For such measurements, high-impact polystyrene (white) or electron solid water are the recommended phantom materials. White polystyrene is recommended over clear polystyrene because it contains titanium oxide, which raises its effective atomic number closer to that of water. The physical characteristics for some electron-solid-water materials are equivalent enough to water so that no correction to depth dose should be necessary. Agreement between depth dose measured in electron solid water and water is within

TABLE VIIIa. Electron fluence ratios for clear polystyrene (Hogstrom and Almond, 1982).

Depth (cm)	Incident energy (MeV) 6	8	10	12	14	16	18	20
0.0	1.000	1.000	1.000	1.000	1.000	1.000	1.000	1.000
0.5	1.008	1.005	1.003	1.002	1.002	1.002	1.001	1.001
1.0	1.020	1.011	1.007	1.005	1.004	1.003	1.003	1.002
1.5	1.038	1.019	1.012	1.009	1.006	1.005	1.004	1.004
2.0	1.070	1.031	1.018	1.012	1.009	1.007	1.006	1.005
2.5		1.047	1.026	1.017	1.012	1.010	1.008	1.006
3.0			1.037	1.023	1.016	1.012	1.010	1.008
4.0				1.041	1.026	1.019	1.015	1.012
5.0					1.043	1.029	1.021	1.017
6.0						1.045	1.031	1.023
7.0							1.046	1.033
8.0								1.047
9.0								
10.0								

TABLE VIIIb. Electron fluence ratios for high-impact polystyrene (Hogstrom and Almond, 1982).

Depth (cm)	Incident energy (MeV) 6	8	10	12	14	16	18	20
0.0	1.000	1.000	1.000	1.000	1.000	1.000	1.000	1.000
0.5	1.007	1.004	1.003	1.002	1.001	1.001	1.001	1.001
1.0	1.016	1.009	1.006	1.004	1.003	1.002	1.002	1.002
1.5	1.031	1.015	1.010	1.007	1.005	1.004	1.003	1.003
2.0	1.056	1.024	1.014	1.010	1.007	1.005	1.004	1.004
2.5		1.038	1.021	1.013	1.010	1.007	1.006	1.005
3.0			1.029	1.018	1.012	1.009	1.007	1.006
4.0				1.032	1.021	1.015	1.011	1.009
5.0					1.034	1.023	1.016	1.013
6.0						1.036	1.024	1.018
7.0							1.037	1.025
8.0								1.038
9.0								
10.0								

TABLE VIIIc. Electron fluence ratios for PMMA (Hogstrom and Almond, 1982).

Depth (cm)	Incident energy (MeV) 6	8	10	12	14	16	18	20
0.0	1.000	1.000	1.000	1.000	1.000	1.000	1.000	1.000
0.5	1.004	1.002	1.001	1.000	1.000	1.000	0.999	0.999
1.0	1.010	1.004	1.002	1.001	1.000	0.999	0.999	0.999
1.5	1.021	1.008	1.004	1.001	1.000	0.999	0.999	0.998
2.0	1.046	1.015	1.006	1.003	1.001	0.999	0.998	0.998
2.5		1.027	1.010	1.004	1.001	1.000	0.998	0.998
3.0			1.017	1.007	1.003	1.000	0.998	0.997
4.0				1.019	1.008	1.002	0.999	0.997
5.0					1.020	1.008	1.002	0.998
6.0						1.021	1.007	1.001
7.0							1.022	1.007
8.0								1.022
9.0								
10.0								

1% (Ho et al., 1985). One cannot, in general, expect the depth dose measured in plastic phantoms to agree with that measured in water unless the data are corrected for effective depth and the fluence factor discussed above. It is recommended that the depth be corrected for the effective density. It is recommended that the central-axis depth-dose distribution be based on ionization measurements in water. By defining the zero depth of the plastic phantom at the appropriate position, it is possible to force the 50% isodensity contour of the film on the central axis to be at the same depth as the 50% depth dose measured using ion chamber dosimetry.

III. ENERGY DETERMINATION

Dose distributions and certain beam parameters depend strongly upon electron energy that must be specified in a meaningful way and determined for each clinical electron beam (Brahme and Svensson, 1976). The electron beam inside the accelerator tube just before hitting the accelerator window is the intrinsic electron beam. This beam has a very small energy and angular spread. As the intrinsic electron beam passes through the exit window, scattering foil, monitor chamber, air, and other materials in reaching the phantom surface, electron energy spread and angular spread are significantly increased.

The most probable energy (kinetic) at the surface, $E_{p,0}$, in MeV is related to the practical range, R_p in cm (for a definition of R_p see below), in water by the simple relationship

$$E_{p,0} = C_1 + C_2 R_p + C_3 R_p^2, \quad (13)$$

where C_1, C_2, and C_3, are constants.

NACP (1981) and ICRU (1984) found that Eq. (13) with $C_1 = 0.22$ MeV, $C_2 = 1.98$ MeV cm^{-1}, and $C_3 = 0.0025$ MeV cm^{-2} reproduces the measured data with an accuracy of 2% from a few MeV to 50 MeV. This task group recommends these values which are valid for broad beams greater than 12 x 12 cm^2 for energies up to 20 MeV and greater than 20 x 20 cm^2 for higher energies, and for SSDs equal to or greater than 100 cm. Recent Monte Carlo simulations using the EGS4 code have generated similar values (Rogers and Bielajew, 1986). A comparison of the various energy-range relationships is shown in Fig. 8.

To be in strict accordance with this formalism, R_p should be determined from measured depth-dose data corrected for beam divergence. However, if one uses depth-ionization data, for SSD> 100 cm and uncorrected for divergence, the difference in R_p is not clinically significant for the calculation of $E_{p,o}$. Therefore, for clinical application this task group takes the position that R_p may be determined adequately from depth-dose or depth-ionization curves with or without divergence correction. The practical range R_p is determined from the depth-dose or depth-ionization curves as the depth of the point where the tangent at the inflection point of the falloff portion of the curve intersects the bremsstrahlung background, as shown in Fig. 10. A broad-beam, narrow-detector geometry should be employed for these measurements. In order to correct for beam divergence, the measured values of dose or ionization at each depth should be multiplied by the factor

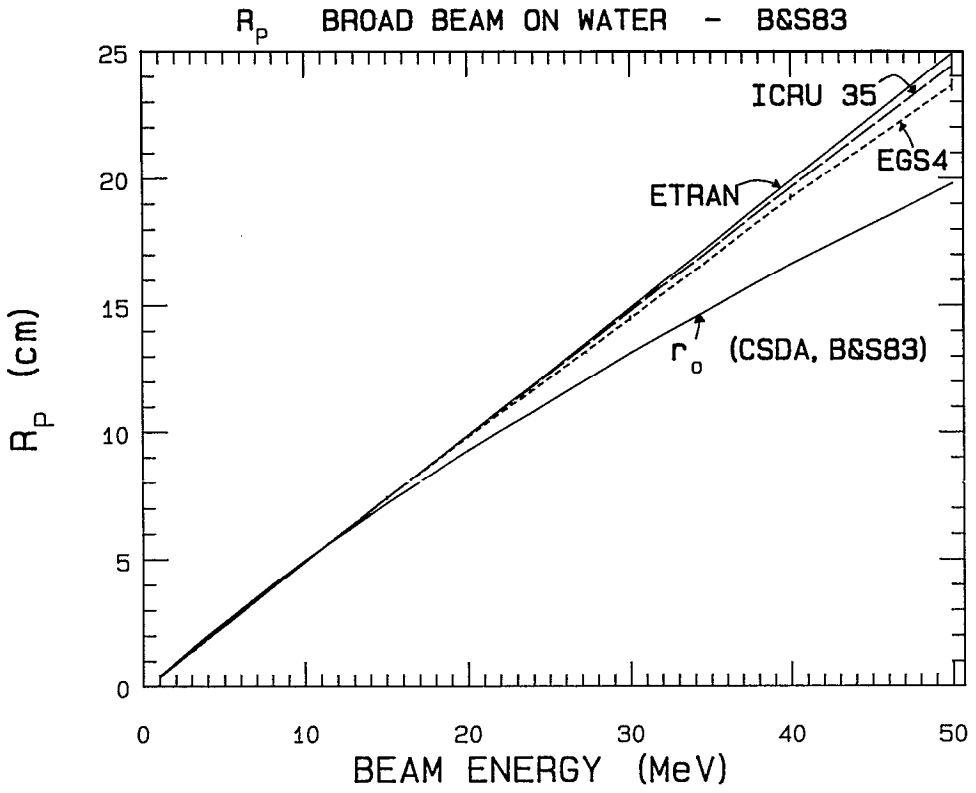

FIG. 8. A comparison of the practical ranges (above the bremsstrahlung tail), R, as calculated with EGS4 and ETRAN using the 1983 stopping powers, as calculated with the empirical formula recommended by ICRU (1984). The curve designated r_0 calculated using the continuous slowing down approximation (CSDA). (From Rogers et al., 1986).

$$\frac{(\mathrm{SSD}_{\mathrm{eff}}+d)^2}{(\mathrm{SSD}_{\mathrm{eff}})^2}, \tag{14}$$

before the determination of range, where $\mathrm{SSD}_{\mathrm{eff}}$ is the effective source-to-phantom distance (see Sec. VIII for details). Because the effect of this correction on dose distributions is small for energies less than 20 MeV, the nominal SSD may be employed in determining this correction factor without a clinically significant loss of accuracy.

Practical range measurements using depth dose are only slightly different (on the order of 1 mm for 30 MeV) from those obtained from depth ionization curves (ICRU, 1984). Practical range measurements in plastics should be converted to those in water by using the scaling factors recommended elsewhere (Sec. II E).

The physicist is aware that the energy spectrum of the high-energy electron beam, unlike that of an x-ray beam, decreases in energy rapidly with depth in the absorbing medium, with a consequent change in stopping power with depth. Nevertheless, the ratio of stopping powers in different media may change little with depth. However, a further phenomenon, the polarization density effect, originally postulated by Fermi for charged particles and shown to be important for high energy electrons, has the consequence that the dose conversion factor for a gaseous ionization chamber in water (or other medium) varies demonstrably with depth. Stopping power tables include this effect (Fermi, 1940; Sternheimer, 1952; Laughlin and Beattie, 1951; Berger and Seltzer, 1968; Zsula et al., 1957).

Several dosimetry protocols recommend the use of the following relationship for the determination of the mean energy of the electron beam at the surface of the phantom, $\bar{E}_0$,

$$\bar{E}_0 = C_4 R_{50}, \tag{15}$$

where C_4 is a constant and R_{50} is taken as the depth of either the 50% ionization or dose levels. The value of C_4 has been controversial and has been studied by Rogers and Bielajew (1986). The original value of 2.33 MeV cm^{-1}, which was employed by the AAPM (1983) and NACP (1981) protocols, was determined by Berger and Seltzer from Monte Carlo transport calculations of plane-parallel broad electron beams. This value was an average for values in the energy range 5-50 MeV and is applicable to the 50% value of the depth-dose curve. Wu et al. (1981) have calculated C_4 for depth-ionization curves and recommend a value of 2.381 MeV cm^{-1} to determine energy from the R_{50} for the depth-ionization curve. Furthermore, if data are not corrected for beam divergence, then a slightly greater value is required. The NACP (1981) protocol, as well as Schulz and Meli (1984), have shown that if one neglects the beam divergence in the determination of the mean energy, the error in dose calibration is less than 1%. However, for more accurate estimates of the mean energy of the beam one should use the data presented in Fig. 9.

Task Group 25 recommends that either the AAPM (1983) protocol value for C_4 of 2.33 or the HPA (1985) protocol value of 2.4 times either the depth of 50% ionization or 50% dose, corrected or uncorrected for divergence, are acceptable for estimating the incident mean energy to be used for the calculation of relative dose. This task group recommends that, within this framework, the physicist select the method consistent with his or her calibration protocol.

For absorbed dose measurements with an ion chamber, it

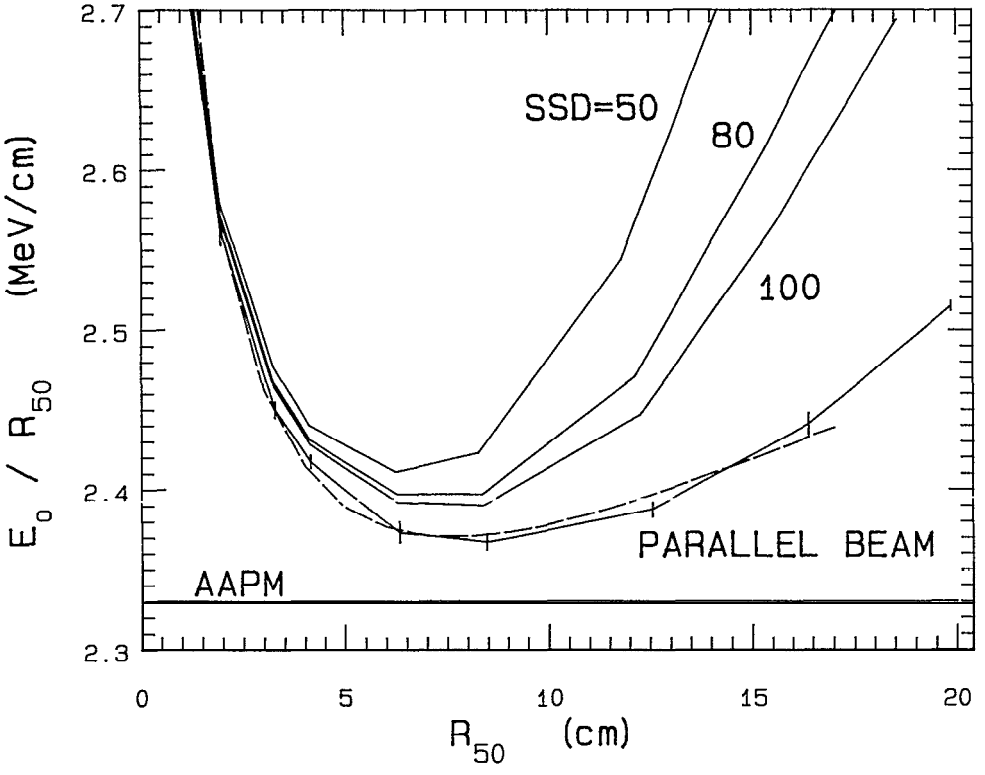

FIG. 9. Values calculated by EGS4 for E_0/R_{50} as a function of R_{50} (depth of 50% dose in water) for various values of source-to-surface distance. The constant value recommended by the AAPM is also shown. The values for the parallel beam case predicted by Eq. (2) in the original paper are shown. (From Rogers *et al.*, 1986).

is necessary to know the mean electron energy $\boldsymbol{E}_d$ at the location of the detector in order to determine the replacement correction (AAPM, 1983). As the electron beam penetrates the phantom, the mean electron energy at a depth d decreases and can be estimated from the linear relationship

$$\overline{E}_d = \overline{E}_0(1 - d/R_p). \tag{16}$$

These energy parameters, $(\boldsymbol{E}_p)_o$, $\boldsymbol{E}_o$, and $\boldsymbol{E}_z$, as well as range parameters $\boldsymbol{R}_p$ and $\boldsymbol{R}_{50}$, are of direct interest in treatment planning, dosimetry, and energy specification. A depth-dose or depth-ionization measurement for every electron-beam energy allows one to obtain all of the above parameters.

IV. BEAM FLATNESS AND SYMMETRY

A. Specification of beam uniformity

Uniformity of intensity across the electron-beam field is a requirement for the therapeutic use of electron fields. Symmetry and flatness of an electron beam are dependent on the design and adjustment of the flattening system and the apparatus used for beam collimation. The electron beam passes through the vacuum window of the accelerator guide, scattering foils, the beam monitoring chambers, the intervening air, and the field-defining apertures. Often electrons are scattered from the cones and x-ray jaws are intentionally used to augment flatness. Because scattered electrons are of lower energy, the flatness of the beams may change significantly with depth. (Lax and Brahme, 1980).

Electron field uniformity can be defined by setting specific recommendations on field symmetry and flatness for a specified area of the beam at depth. The reference depth used for this determination has traditionally been at or close to the depth of maximum dose. It is recommended that the uniformity also be evaluated near the surface and at the therapeutic range (defined in Sec. V). The measurements should be made on each of the principal and diagonal axes of the beam for the largest field for each applicator. Flatness specifications should be checked at several collimator angles at several gantry angles.

A reference plane is defined as a plane parallel to the surface of the phantom and perpendicular to the central axis. Since the depth-of-dose maximum varies significantly between different machines, we recommend that the reference plane be at the depth of the 95% isodose beyond the depth-of-dose maximum. The variation in the dose normalized to the central-axis value should not exceed ± 5% (optimally be within ± 3%) over an area confined within lines 2 cm inside the geometric edge of fields equal to or larger than 10X10 cm.

In regard to beam symmetry, the cross beam dose profile in the plane of reference should not differ more than 2% at any pair of points situated symmetrically, with respect to the central ray.

B. Measurement of beam flatness and symmetry

One of the most frequently used dosimetry systems for determining field uniformity is film. Using film, both flatness and symmetry can be evaluated for an electron field in a relatively short time. The film is irradiated at depth in a solid phantom, positioned perpendicular to the beam axis. Films should be exposed at several different collimator and gantry

positions to verify that field uniformity does not change. All applicators and energies should be evaluated.

Measurements made in water phantom with small ionization chambers or diodes can also accurately determine the beam symmetry and flatness, but these measurements cannot easily be done for gantry angles other than for 0° and ±90°. Measurements with ionization chambers and automatic scanning devices can be done quickly, and often the entire reference plane can be evaluated. However, some automatic devices cannot be used easily with accelerators that employ scanning electron beams. Other systems, such as those that use film, that integrate the dose for the entire scanned field are necessary.

In those cases of electrons scattered off the beam-defining systems, changes in the beam-defining aperture of the cone applicator, or trimmers, can change flatness (Lax and Brahme, 1980). Therefore, the effects of custom blocking should be evaluated to insure that the electron field flatness and symmetry have not been changed significantly.

Beam flatness and symmetry are evaluated at the time of machine installation and should be subsequently verified at least weekly and following any major servicing of the accelerator (e.g., wave guide, gun, bending magnet, scattering foils, etc.). Frequent verification of beam flatness and symmetry is part of any good quality assurance program.

V. PERCENT DEPTH DOSE

Electron fields are most often used clinically with fixed SSD techniques. Only occasionally are isocentric techniques used. This section will deal with only fixed SSD dosimetry.

Percent depth-dose measurements for electron beams should be performed for each available energy for the range of field sizes available. Small differences in energy, scattering foils, or scanning systems can affect the electron-beam characteristics (Almond, 1981; Kirby ***et al.,*** 1985). During acceptance testing procedures the central-axis depth-dose curves should be evaluated and compared to the specifications. Often during these initial tests the energy of the electron beam must be adjusted to meet individual specifications.

In accordance with ICRU (1984) recommendation it is recommended that several parameters be used to characterize the electron central-axis depth-dose curve (Fig. 10). The parameters, $\%D_s$, $\%D_x$, R_q, R_{100}, R_{50}, R_p, and G_0, are defined as follows.

(i) The relative surface dose $\%D_s$, is defined at 0.5-mm depth. This depth has been recommended because of the difficulty of obtaining accurate dose measurements at an air phantom interface. In addition the sensitive layers of the epidermis are approximately at this depth in tissue.

(ii) All electron beams have an x-ray component that is dependent on the energy of the beam and the design of the accelerator. The relative dose due to the x-ray component, $\%D_x$, is extrapolated from dose measurements beyond the maximum range of the electrons.

(iii) The therapeutic range R_q is used as a measure of the clinically useful portion of the electron depth-dose profile. This task group recommends the depth of the deepest 90% dose level as the therapeutic range R_{90}.

(iv) R_{100} is the depth in water of the dose maximum and depends on field size and the angular and energy distribution of electrons at the surface. R_{50}, is the depth of the 50% dose level and R_p, is the practical range (defined in Sec. III).

(v) The normalized dose gradient G_0, is a measure of the steepness of the descending portion of the depth-dose curve. It is defined as the ratio of the R_p, to the difference between R_p, and R,, where R_q, is the depth at which the tangent to the curve at the point of inflection meets the level of D_{max}, as shown in Fig. 10.

A comparison of several of these parameters for various machines is given in Tables IX and X.

A. Surface dose

The surface dose ***%D.,*** defined at 0.5-mm depth on the central axis, should be determined for all energies and for the full range of clinically used treatment fields. To measure dose near the surface, a thin-window plane-parallel chamber is required and measurements are typically made in a solid phantom. Thin TLD chips can also be used. Film should only be used perpendicular to the beam axis.

Surface dose varies with energy, being less at the lower energies, e.g., 74% at 7 MeV and 87% at 15 MeV (Meyer et al., 1984). For small fields the central-axis depth-dose curve appears shifted towards the surface, with an increase in dose in the buildup region. Changes in collimator to surface distances can also modify the buildup region, including the dose at the surface. Figure 11 indicates the variation of surface dose with energy of the electron beam, showing that the relative dose increases with beam energy. It also shows the strong dependence on machine type, which results from the methods used to flatten and collimate the beam.

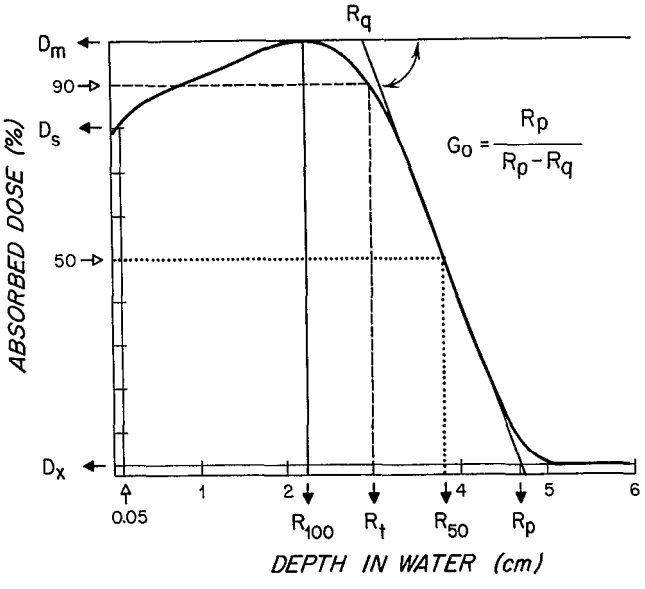

FIG. 10. Central-axis depth-dose curve for an electron beam with parameters indicated that can be used to characterize electron beams. The therapeutic range is at the 90% depth dose level as recommended by this task group all other parameters as discussed in ICRU (1984).

TABLE IX. The electron beam characteristics for various linear accelerators measured by Kirby et al., (1985) where N is the number of treatment units from which the data was determined. (Energies in MeV, distances in mm).

Machine model	E_{nom}	$\bar{E}_0$	$E_{p,0}$	N	R_{max}	R_{99}	R_{95}	R_{90}	R_{80}	R_{50}	R_{20}	R_p
Clinac 18	6	5.4	...	2	...	...	...	...	18	23	...	...
	9	7.7	8.6	5	16	13–20	23	24	27	33	38	41
	12	10.5	11.7	14	22	16–26	31	34	37	45	52	57
	15	13.3	14.3	5	21	15–29	37	42	47	57	66	71
	18	...	...	2	...	...	...	...	58	...	...	...
Clinac 20	6	5.4	6.3	2	10	8–12	14	16	19	23	27	29
	9	8.2	9.4	4	16	11–19	23	26	29	35	41	45
	12	10.5	11.5	6	22	18–25	30	34	38	45	51	56
	16	14.2	...	2	...	...	...	...	54	61	...	...
	20	19.1	...	2	...	...	...	...	64	82	...	...
Clinac 35	10	9.3	10.3	1	20	15–23	...	28	33	40	...	50
Mevatron 12	6	5.1	...	3	...	...	...	...	18	22	...	...
	7	6.1	...	3	11	...	19	22	23	26	...	...
	8	7.0	8.0	5	15	12–17	20	22	25	30	35	38
	10	8.9	...	1	...	...	...	...	32	38	...	...
	11	9.6	10.7	4	22	18–25	28	31	35	41	48	52
	12	11.0	11.9	3	28	24–30	35	38	41	47	55	58
Mevatron 20	7	6.3	7.1	2	15	12–16	17	21	23	27	30	33
	10	9.1	9.7	3	23	19–25	28	30	33	39	45	47
	12	10.7	11.9	3	27	22–31	34	37	40	46	54	58
	15	14.0	...	2	28	...	...	46	50	60	...	...
	18	16.3	17.0	2	13	4–22	37	47	59	70	81	85
Therac 20	6	5.1	...	1	...	...	...	...	18	22	...	...
	9	8.4	9.0	4	22	20–26	25	28	31	36	41	43
	13	11.7	12.2	3	31	26–34	37	40	44	50	57	60
	17	15.8	...	2	...	...	...	...	60	68	...	...
	20	19.1	...	1	...	...	...	...	71	82	...	...
Sagittaire	10	9.3	10.1	2	24	20–27	30	32	35	40	46	49
	13	12.3	13.0	1	30	29–33	39	41	45	53	60	64
	16	14.2	14.3	1	38	30–42	46	48	52	61	67	71
	22	21.4	21.6	2	38	30–51	64	70	78	92	104	109
LMR 13	8	6.8	7.8	1	15	13–17	19	21	24	29	35	37
	10	...	...	1	...	...	...	...	33	...	...	...
	12	...	...	1	...	...	...	...	39	...	...	...
	13	...	...	1	...	...	...	...	43	...	...	...
SL75	8	7.2	...	1	...	...	...	...	27	31	...	...
	10	8.4	9.6	2	18	?–20	24	26	28	36	41	46
	12	10.7	12.0	2	21	19–26	31	34	41	46	54	59
Allis-Chalmers	8	...	...	1	...	...	...	...	26	...	...	...
Betatron	9	7.5	9.0	1	18	14–20	23	24	26	32	38	43
	10	8.4	9.4	3	17	12–20	23	26	29	36	42	45
	12	10.7	12.2	2	13	9–18	25	29	34	46	54	60
	14	...	...	1	...	...	...	...	42	...	...	...
	15	11.9	13.4	1	15	8–22	28	33	40	51	60	66
Brown-boveri Betatron	10	10.0	10.9	2	21	16–28	28	33	36	43	49	53
Siemens	12	11.0	11.9	1	25	19–28	34	36	40	47	53	58

When electron beams are used to treat superficial lesions, bolus may be required to increase the dose at the surface. A variety of materials have been used as tissue substitutes. The material used should be of low atomic number and have stopping and scattering powers similar to water. Paraffin wax, polystyrene, and acrylic are some of the materials typically used (Sharma ***et al.,*** 1983). Other commercial materials are available, but all materials should be evaluated by comparing the depth dose in the bolus material relative to water. All bolus material should be placed directly on the patient's surface.

B. X-ray background

There is an x-ray component with all electron beams due to bremsstrahlung interactions between the electrons and the accelerator end window, scattering foil, ionization chambers, collimation system, and the patient (ICRU, 1984; Lanzl, 1982). The x-ray component of the beam increases with the energy of the electron beam. Accelerators with scanning beams should have a smaller x-ray component than those utilizing a scattering foil, especially at high energies (Brahme and Svensson, 1976) (Fig. 12 and Table X). For single-field treatment techniques at energies below 10 MeV

TABLE X. Comparison of the electron beam characteristics for several accelerators with nominal 20-MeV beams. G_0 is the reduced dose gradient and the theoretical data is from Brahame and Svensson (19761, Almond, P. R. (1981).

Machine	R_p (cm)	$\hat{E}_0$ (MeV)	G_0	R_{85} (cm)	R_{50} (cm)	$\bar{E}_0$ (MeV)	D_x (%)
Theoretical	10	19.9	3.4	7.3	8.5	19.8	1
Therac 20 (traveling wave scanning magnet)	10	19.9	3.1	7.3	8.4	19.5	2.7
Microtron (two foil)	10	19.9	2.94	7.0	8.4	19.5	2.7
Asklepitron 45 (Betatron two foil)	10	19.9	2.9	6.4	8.2	19.1	3.5
Clinac 20 (standing wave two foil)	10	19.9	2.6	6.1	8.2	19.1	6.0
SL75-20 (traveling wave single foil)	10.1	20.1	2.4	6.0	8.2	19.1	6.0
Mevatron 77 (standing wave two foil)	8.9	17.8	2.9	6.0	7.4	17.2	4

the dose due to x rays is usually less than 3% and for energies above 40 MeV can be as large as 10%.

The determination of dose due to x rays, D_x, is made by extrapolating the bremsstrahlung tail to R_p. Its value can be estimated by measuring ionization at 2 cm and at 4 cm beyond R_p. Normally this measurement is made with an ionization chamber and is indicated as a percentage of the maximum ionization. Changes in field size and air gap can affect the amount of x-ray contamination levels.

The x-ray background is an especially important consideration in the planning of total skin irradiation such as that used in the treatment of mycosis fungoides. If multiple beams or arc therapy is planned, the total x-ray dose near the intersection of the central axes beyond the range of the electrons can be significant.

C. Field size dependence

Electron depth-dose curves depend on the size and the shapes of the treatment fields. The dependence of depth dose with field size is due to the lateral scattering of electrons. This concept is illustrated in Sec. VII and discussed in more detail by ICRU (1984). The central-axis depth-dose curve does not significantly change if the distance to any of the field edges (radius) is greater than one-half of the electron range (ICRU, 1972). As the energy of the electron beam increases, the changes in the central-axis depth-dose curve with field size become more pronounced (ICRU, 1984; Meyer *et al.*, 1984; van de Geijn *et al.*, 1987). The traditional

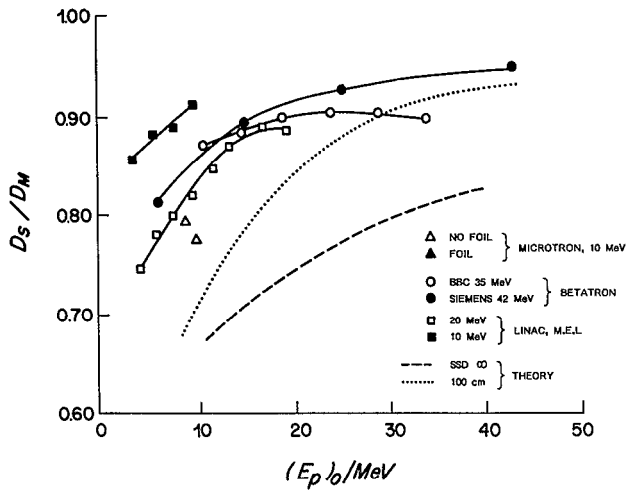

FIG. 11. The variation of the ratio of the surface dose to the dose maximum as a function of energy. Measured ratios are for a number of accelerators and theoretical calculations redrawn from Brahame and Svensson (1976).

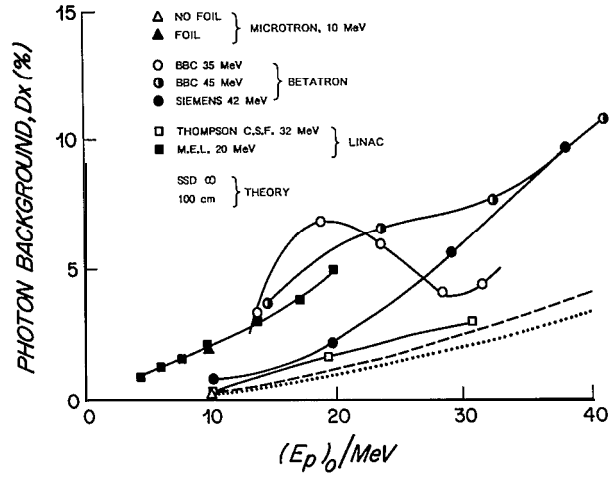

FIG. 12. The photon background increases with energy and can be as high as 10% of the dose at depth maximum; the photon dose changes with the type of accelerator. Additional data for a number of other accelerators can be seen in Tables IX and X. Figure is redrawn from Brahame and Svensson (1976).

concept of equivalent square fields as applied to photon beams does not apply to electron beam depth-dose data (Fig. 13). Also, the smaller the field, the greater is surface dose and the shift of d_{max} and R_{90} towards the surface (Fig. 14).

Hogstrom ***et al.*** (1981) have shown that the central-axis depth-dose curves for rectangular fields of size ***X*** and ***Y*** can be determined by taking the square root of the product of the depth doses for the square fields whose sides are ***X*** and ***Y:***

$$\%D^{X,Y}(d) = [\%D^{X,X}(d) \times \%D^{Y,Y}(d)]^{1/2}. \quad (17)$$

The above equation can be rearranged for measuring the dose on the central axis for small fields (Meyer et al., 1984), i.e.,

$$\%D^{X,X}(d) = \frac{[\%D^{X,Y}(d)]^2}{\%D^{Y,Y}(d)}. \quad (18)$$

For example, the depth dose for a 2x2 cm^2 field size can be determined from the measurement of the depth doses for a 2X10 cm^2 and a 10x10 cm^2 field. In application of Eq. (17) and Eq. (18) it will be necessary to normalize the results so that the maximum value of the ***%D*** is 100% for each field size, if one's clinical convention is to normalize all depth doses to 100% at the maximum dose value on central axis.

A number of authors have proposed methods using computer techniques for calculating the central-axis depth-dose curves for irregularly shaped electron beams (Hogstrom and Almond, 1981; Werner et al., 1982; Bruinvis, 1985). For irregularly shaped electron fields the depth dose depends primarily on the shape of the field surrounding the point of interest. However, small changes in large electron fields, such as trimming the comers of a field, will not modify the dose in the central portion of the field. All irregularly shaped fields that have large areas of the field removed, such as "L-shaped" fields, require additional measurements of the depth dose. (For highly irregular fields, the conventional central axis may lie beneath the blocked area.)

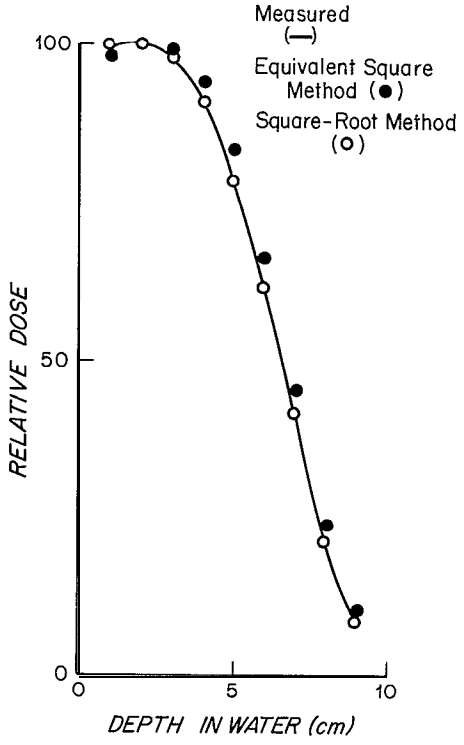

FIG. 13. The measured central-axis depth dose of a rectangular field compared to calculations of the depth dose using the square-root method proposed by Hogstrom et al. (1981). The solid points were determined using the equivalent-square method used in photon dosimetry and the error that would be made using this method. Field size, 3X8 cm, electron energy, 18 MeV. Redrawn from Meyer et al. (1984).

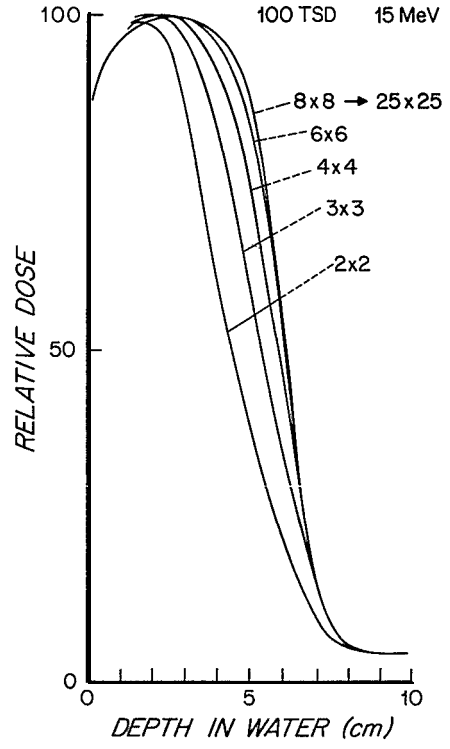

FIG. 14. Central-axis depth-dose curves for a number of field sizes demonstrating the decrease in dose at depth for small fields on the Siemens Mevatron 80 15 MeV. Redrawn from Meyer et al. (1984).

D. Measurement of depth-dose curve

Measurement of ionization in water using small cylindrical chambers is by far the most common method of determining the dose at depth in an electron beam. The procedures recommended by this Task Group for determining central-axis depth-dose curves from ionization chamber measurements are given in detail in Sec. II A. In some cases, other methods of measuring the central-axis depth-dose curve, such as with film, diodes, and TLDs may be more convenient than ionization chamber measurements. However, these measurements should be compared to the data obtained with ionization chambers in water or solid phantoms. See Sec. II regarding the use of the above dosimeters. At each energy, a set of depth-dose curves versus field size should be measured sufficient to permit linear interpolation to other field sizes. The measurement of the central-axis

depth-dose curve for small fields requires the use of small volume ionization chambers to insure that the collection volume is within the uniform dose region (Sharma *et al., 1984).* The technique described by Eq. (18) can also be used to derive data for small fields from larger fields. The direct measurement of very small fields, maximum dimensions 3 cm or less, requires the use of other detectors such as film and TLDs. Figure 15 shows the change in depth as a function of beam area for square fields for the 80% depth dose for electron beams with nominal energies from 4 to 18 MeV (Biggs *et al., 1979).*

VI. DOSE DISTRIBUTIONS

For treatment planning with electrons, measured dose distributions in water for each individual machine must be available. The dose distributions for selected square, circular, and rectangular fields should be measured in a plane defined by the central axis of the beam and one of the principal transverse axes.

Dose distributions serve the following purposes: (i) Visualization of dose distributions for patient planning; (ii); input for hand-calculated or computer-calculated patient dose distribution; (iii) provide data to check the accuracy of computer generated dose distributions; and (iv) documentation of treatment beams for subsequent quality control or comparison with treatment beams of other accelerators.

A. Characterization of dose distributions

A dose distribution for a particular field in water can be characterized by its central-axis depth-dose curve (see Sec. V) and by its off-axis ratios and by an isodose chart. The off-axis ratio at a point is defined as the ratio of dose at that off-axis point to the dose on the central axis at the same depth. It is recommended that isodose curves be plotted with 100% equal to the maximum dose on the central axis for the following set: l00%, 95%, 90%, 85%, 80%, 70%...20%, 10%, and every 5% above 100%. It is useful to plot the 5% and lower isodose levels in order to show the bremsstrahlung dose contribution and any collimator leakage.

The depth-dose parameters, $\%D_s$, R_{100}, R_{90}, and G_0, as discussed in Sec. V, and off-axis parameters such as penumbra width and flatness can be extracted from the dose distribution. Of particular importance is the shape of the 90% isodose curve for evaluation of the coverage of a target volume. All isodose curves are needed for the evaluation of dose with respect to critical structures. In Fig. 16, the 90% isodose curve (treatment volume) is compared with the shaded volume defined by the projection of the field edge and the therapeutic range. At R_{100}, the 90% isodose is located approximately 1 cm inside the geometric edge. In the corners of the shaded volume at the therapeutic depth, note that the relative dose value is only about 50%. The characterization of the dose falloff in the lateral dimension (penumbra) is particularly useful in calculating the dose distribution in the region of field abutment and for evaluating the dose with respect to normal tissues outside the target volume.

For different machine designs, electron energies, and air gaps, the shapes of isodose curves vary. Table XI lists qualitatively the expected variation in beam characteristics. For example, if one compares the isodose distributions of a beam broadened using a scattering foil system versus a scanning magnet, one typically finds the following: (i) Increased surface dose for a beam with a scattering foil; (ii) decreased depth-dose gradient due to increased energy spread and angular spread of the electrons exiting the foil (ICRU, 1984); (iii) shallower therapeutic depth, also due to the increased energy spread; and (iv) increased bremsstrahlung dose due to the x-ray production in the foil.

These differences are most significant for machines using single scattering foils at higher energies. The newer machines using dual scattering foils give dose distributions that are more similar to those of the scanning beams. In evaluating collimation systems, one should be aware that compared to trimmers, treatment cone generates scattered low-energy electrons.

As the beam energy increases

(i) the surface dose increases due to a slower build-up of dose with depth as a result of decreased multiple Coulomb scattering, (ii) the dose gradient decreases because the increased depth of penetration gives the beam a longer path

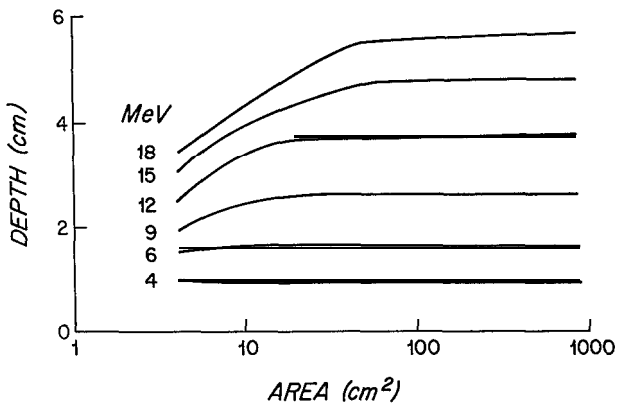

FIG. 15. The modification in the depth of the 80% depth dose due to the change in the square area of the electron field for six nominal energies on a Varian Clinac 18. Redrawn from Meyer et al. (1984).

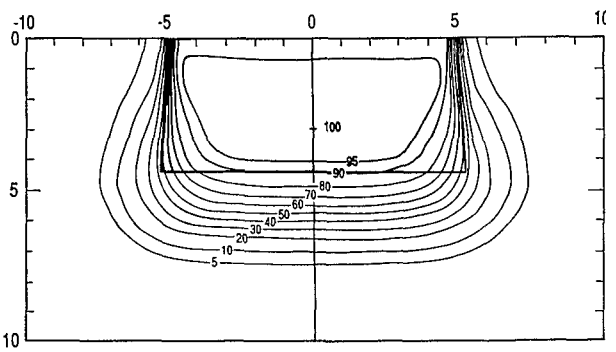

FIG. 16. Isodose distribution for a 10-cm² field, 115 MeV electron beam on a Siemens Mevatron 77. The shaded area is defined by the edge of the geometric field and R_{90}. Note the lateral constriction of the 90% isodose curve with depth. From K. R. Hogstrom [personal communication].

TABLE XI. Qualitative differences in characteristics of isodose curves effect on dose parameters for varying beam conditions. 0 = minimal variations, + = moderate increase, + + = significant increase, − = moderate decrease.

	Surface dose, D_s	Depth to 90% R_{90}	Dose gradient, G_0	Bremsstrahlung dose, D_x	80%–20% Penumbra at surface	80%–20 Penumbr depth of
Scatter foil versus scanning beam	+	−	−	+	0	0
Cone versus trimmers	+	−	−	+	0	0
increasing energy	+	+	−	+	+	+
Increasing air gap (~10cm)						
Low energy (≤6 MeV)	0	0	0	0	+ +	+ +
High energy (≥10 MeV)	0	0	0	0	+ +	+

length in which to become diffused due to multiple scattering, (iii) therapeutic depth and bremsstrahlung dose both increase approximately linearly with energy, (iv) the penumbra at the surface decreases because of the decreased scatter in air with increasing electron energy, and (v) the penumbra at the therapeutic depth tends to increase because the longer path length allows the beam to become more diffused due to multiple scattering.

As the air gap between the collimator and the phantom surface increases, the penumbra for low-energy beams increases proportionately due to scatter in the intervening air space. For higher energy electron beams, the penumbra is largely due to scatter in the phantom and, therefore, the effect of the air gap is less.

B. Measurement of isodose curves

Isodose curves for a 10x10 cm^2 field size or a standard field size should be measured at each energy. Additionally, isodose curves for the full clinical range of field sizes (>3X3cm^2) should be measured. If treatments at nonstandard air gaps are used, isodose curves should also be measured either for a complete set or for selected field sizes to verify calculational algorithms.

Isodose curves can be measured directly by an isodose scanner or constructed from a matrix of measured dose points. If the isodose scanner uses an energy-dependent probe (e.g., ionization chambers), depth-dependent corrections should be incorporated into the system. The probe may provide an instantaneous reading (e.g., ionization chamber or silicon diode) or one to be read later (e.g., film). If the beam is spread by a scanning magnet, the beam must be sampled either synchronously (Ertan ***et al.,*** 1984) or for times as long *as* one minute to achieve 1% to 2% accuracy, making the operation of isodose tracking devices impractical, except for the case of reading film. Film dosimetry, which offers a convenient method of obtaining a complete set of isodose curves, is discussed in Sec. IID. Film methods are attractive for scanning electron beam machines when the scan period is long or for applications where data acquisition time is limited.

The more common method of measuring dose distributions is by recording data on a regular grid of locations, converting the readings to dose, and then plotting isodose curves. Another method of measuring the isodose distribution is to measure the central-axis depth-dose curve and the off-axis profiles separately. The off-axis profiles should be measured at several depths, which should include as a minimum the following: (i) Depth at or near the surface; (ii) depths of 90% and 20% dose; (iii) depth 1 cm beyond the practical range; and (iv) two or more depths equally spaced between the surface and depth of 90% dose.

From this set of data, linear interpolation is then usually sufficient for the construction of isodose curves.

It is emphasized that although the discussion above relates to a single plane, it will be desirable for many treatments to obtain the analogous data for other planes that do not necessarily include the central axis. These other data are necessary for the development of a three-dimensional distribution of the dose in the irradiated volume.

VII. OUTPUT FACTORS

The dose per monitor unit (output) is a function of field size. Formalisms for characterizing output depend upon accelerator design and in particular on how the manufacturer chooses to flatten and collimate the fields. For machines with applicators, measurements of electron beam output as a function of field size are necessary for each applicator and each electron energy; therefore, the total number of output measurements is usually quite substantial (Khan *et al.,* 1976; Goede *et al.,* 1977; Choi *et al.,* 1979; Biggs *et al.,* 1979; Purdy *et al.,* 1982).

Regularly shaped electron fields are obtained by one of two methods. For most accelerators a set of applicators or cones are provided that are attached to the head of the machine. When an electron cone is inserted on most medical accelerators, the x-ray collimators open automatically to a field size preset by the manufacturer. This setting may be a function of energy. However, on some older units it may be necessary to manually adjust the x-ray jaws. In either case, for each cone, the machine should be interlocked for only one x-ray collimator setting. The manufacturer will usually supply a number of cones and may also provide inserts for the cones that cover a range of field sizes and standard shapes: square, circular, or rectangular. Alternatively, on some accelerators, a set of trimmer bars synchronously track the x-ray collimators to produce a continuous set of field

sizes. A hybrid method of producing a continuous range of field sizes is to attach a variable collimator, which by appropriate adjustment, may produce any square or rectangular field.

The output factor OF (F) is defined as the ratio of dose per monitor unit U at d_{max}, for a given field size F to that for the reference field size at its own $d_{max,o}$. The dose per monitor unit, $D/U(F,d_{max})$, is given by the following relationship:

$$D/U(F,d_{max}) = \text{OF}\ (F) \times D/U\ (F_0, d_{max,0}), \qquad (19)$$

where F_0 is the reference field size.

The dose deposited at d_{max} depends upon electrons that travel by a number of paths. (i) Some electrons come directly from the source (undergoing only scattering in the intervening air and phantom), (ii) others are scattered from the x-ray jaws, and (iii) others are scattered from the cones or trimmers.

Which of these factors contributes most to the change of output with field size depends upon energy, the collimator design, and field size. For example, with small fields the dose per monitor unit at d_{max} decreases as the field size is reduced primarily because of the lack of side scatter equilibrium in air and in phantom. This leads to a reduction in the output factor. For large fields, the reduction in output with field size is mainly due to a decrease in scatter from the x-ray collimators. For a particular cone with different inserts the variations in output are due predominately to (i) and (ii).

The concept of side-scatter equilibrium is important in electron-beam dosimetry (it should be understood that once a point begins losing side-scatter equilibrium, it can be considered to lie in the penumbra of the field. Therefore, one should be extremely careful in understanding the dose distribution for small field sizes or extended treatment distances. This effect is most significant at low electron energies, since the angular scattering power for electrons is approximately inversely proportional to the square of the energy), as is the concept of equilibrium of secondary electrons in the dose build-up of x-ray beams. The principle of side-scatter equilibrium is different and can be understood quantitatively using Fig. 17. Any electron passing through the final beam-defining collimator has a probability of reaching a particular point in the phantom. The probability is a function of (i) the location of the electron as it passes through the collimator, (ii) the angular distribution of the electrons at that point, and (iii) the probability that the particle will be scattered such that it will arrive at the point of interest. In Fig. 17 (a) it is seen that the spatial distribution of electrons at the collimator that reach a point at the depth of maximum dose is approximately Gaussian in shape. If most of these electrons (e.g., > 99%) reach the point of interest, then side-scatter equilibrium is said to exist. Such is the case in Fig. 17 (a). In Fig. 17(b) it is seen that if the collimator closes sufficiently, then some electrons that could have reached the point of interest are removed from the beam. In this case, side-scatter equilibrium does not exist, and one observes a decrease in the output factor due to field size.

In Fig. 17 (c) the spatial distribution of electrons reaching a point at a greater depth (e.g., R_{80}) is seen to be broader

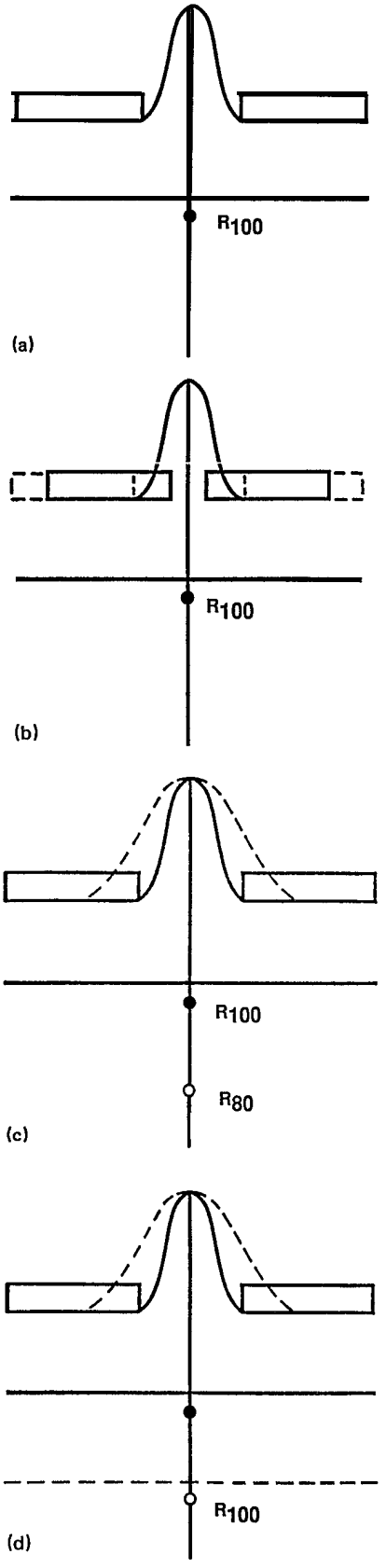

FIG. 17. (a) The Gaussian shaped profile illustrates the probability distribution at the collimator of electrons reaching a point at R_{100}. This geometry represents the standard field size and standard SSD. (b) Same plot as Fig. 17(a), but with the field size reduced. (c) Same plot as Fig. 17(a), but with the dashed profile illustrating the probability distribution at the collimator of electrons reaching R_{80}. (d) Same plot as Fig. 17(a), but with the dashed profile illustrating the probability distribution at the collimator of electrons reaching R_{100} at an extended SSD (dashed surface).

than that for the point at R_{100}. This is primarily due to multiple Coulomb scattering in the phantom. As the collimator closes, the point at the deeper depth is influenced first, losing side-scatter equilibrium, which results in a decreased percentage depth dose. This explains the field size dependence of the depth-dose curve (Fig. 14). When this occurs, the position of d_{max} can shift towards the surface. If the position of d_{max} changes it must be accounted for when measuring output factors. One technique is to measure the dose per monitor unit with the chamber positioned at d_{max} for each field size. Another is to leave the chamber at a reference depth for all field sizes and then modify the dose per monitor unit by the depth-dose curve. In Fig. 17 (d) the spatial distribution of electrons reaching the depth of maximum dose for an extended treatment distance is compared to that of Fig. 17(a). This explains the major reason for the output decreasing faster than inverse square of the distance from the virtual source for small fields at extended treatment distances.

The change in dose per monitor unit as the x-ray collimator settings are varied is demonstrated in Fig. 18 for a fixed cone size (Biggs, 1979); and has also been demonstrated for a trimmer system (Mills *et al.*, 1982). The change in output factor with jaw setting is most marked for low-energy beams where the angular scattering power is greatest. For example, at 4 MeV the output increases by a factor greater than 2 in going from the small to the large jaw settings. This variation is primarily due to lack of side-scatter equilibrium from electrons originating at the level of the x-ray jaws and secondarily due to scattering from the x-ray jaws. The variation in output with jaw setting is much less substantial at higher energies, and the scattering off the x-ray jaw becomes of more relative importance.

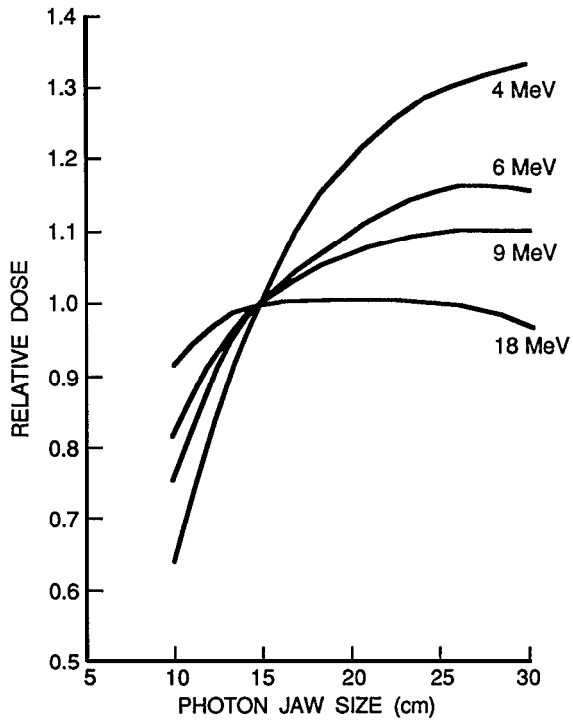

FIG. 18. Change in dose for a fixed number of monitor units as a function of photon jaw size for a single cone. Redrawn from Biggs, 1979.

For most accelerators, scatter from the cones provides a small contribution to the dose at d_{max} and even less so for trimmers. As the energy is increased this contribution is reduced for larger field sizes owing to the reduction in mean electron scattering angle from the cones or trimmers. Thus, these electrons provide a proportionally lower contribution to the dose at d_{max}. Therefore, the introduction of inserts in electron collimators, as long as the field size is large enough for side-scatter equilibrium, will only cause a small change in the output. However, measurements are necessary since it has been reported that for some systems as much as 25%-*40%* of the dose at d_{max} is provided by the scatter from the cones (Loevinger *et al.*, 1961; Briot *et al.*, 1973).

A. Cone or applicator systems

It is recommended that output measurements be made for all standard cone, insert, and jaw setting combinations. In addition, if the cones accept additional inserts, measurements must be made over the range of inserts to be used clinically. With sufficient data it should be possible to obtain output factors for other clinical field sizes of regular shape by interpolation.

The output factor depends upon the cone (or applicator) size (C_s) and the insert size (I_s). Based upon the previous discussion the output factor in Eq. (19) may be written as

$$\mathrm{OF}(F) = \frac{D/U(C_s,I_s)}{D/U(C_0,I_0)}, \tag{20a}$$

which is equivalent to

$$\mathrm{OF}(F) = \frac{D/U(C_s,I_0)}{D/U(C_0,I_0)} \times \frac{D/U(C_s,I_s)}{D/U(C_s,I_0)}, \tag{20b}$$

where the first term of Eq. (20b) is the dose per monitor unit ratio between a cone of size C_s and the reference cone C_0; this term is sometimes called the open cone ratio. The second term is the dose per monitor unit ratio between a cone with an insert and the same cone with its reference insert (open cone). Often the cone insert ratio, Eq. (20a) is measured directly.

The output data for each energy may be presented in a number of ways including

(i) a table of dose per monitor unit at d_{max} for each cone and insert combination,

(ii) a table or graph of output factors as a function of the cone and insert combinations and the dose per monitor unit for the reference field, and

(iii) a table of monitor units necessary to deliver a given dose at a particular isodose level for each cone and insert combination.

For any of these methods it would be particularly useful if output factors could be represented as a function of an equivalent square field size. Biggs (1979) has shown this to be sufficiently accurate for clinical use for a particular accelerator. Shown in Fig. 19 are cone insert ratios for a 6×6 cm^2 cone as a function of equivalent area, where the reference is

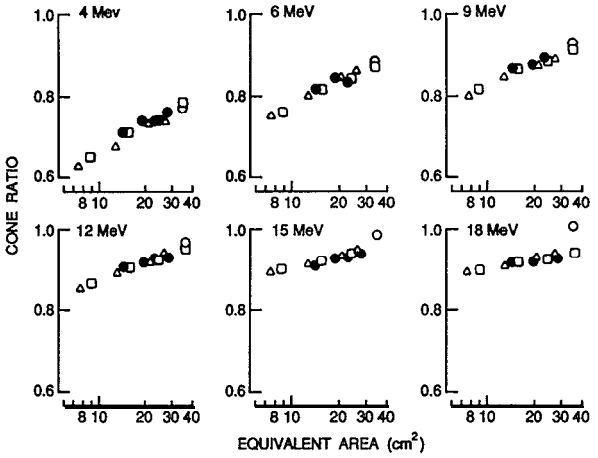

FIG. 19. Cone ratios for 6×6 cm cone as a function of energy. O-Open cone; O-square insert; *-circular insert; n-rectangular insert. Redrawn from Biggs, 1979.

an open 10×10 cm^2 cone. By smoothing the data, Biggs showed that it was possible to obtain the cone ratio to within 2% using equivalent areas. This would not be true for rectangular fields with high aspect ratios.

It must be remembered that the cone ratio depends highly upon the x-ray collimator setting and will differ between machines even of the same manufacturer. For example, on the early Clinac-18, the x-ray jaws were always set 5 cm greater than the cone size. While on the more recent Clinac-18, or Clinac-20, the x-ray collimators are set to a different pattern, which leads to a discontinuous change of output with cone size. This is shown in Fig. 20 where the output factors for a Clinac-20 are plotted for various energies (Purdy ***et al.,*** 1982).

On some machines, extension cones for small field sizes are available. In this case, there is a very large decrease in dose output due not only to the increased SSD, but also the small cone size because of the loss of side-scatter equilibrium.

B. Variable trimmer systems

For variable trimmer systems in which the photon jaws track the trimmers, dose per monitor unit varies smoothly with field size. This is shown in Fig. 21 (Mills, 1985) where the output factor for the Therac-20 is plotted versus the side of the square field. It is important to note that for rectangular fields the dose per monitor unit depends upon which pair of jaws produces the length and width. This is possibly due to backscatter of the electrons from the jaws into the monitor chamber and the different collimator geometry seen by the measurement chamber.

The Gaussian scatter model for pencil beams has been used to develop a formula for the determination of the output factor for any rectangular field from a small set of measured data for the Therac-20 (Mills, 1985). The, ontput factor for a rectangular field produced by scanning beams can be represented by one of the two following equations:

$$\mathrm{OF}(X,Y) = [\mathrm{OF}(X,X)\times\mathrm{OF}(Y,Y)]^{1/2} \quad \text{(square root method)} \tag{21}$$

$$\mathrm{OF}(X,Y) = [\mathrm{OF}(X,Y_0)\times\mathrm{OF}(X_0,Y)] + \mathrm{CF}(X,Y) \quad \text{(one-dimensional method)}, \tag{22}$$

where X_0 and Y_0 are reference field dimensions and CF is a correction factor that accounts for differences primarily due to scatter off the x-ray jaws. Equation (21), called the square root method, predicts rectangular output factors and is accurate to within approximately 3%. This method is least accurate for large fields with large aspect ratios, e.g., 30×10 cm', and cannot distinguish between the different outputs of the two possible orientations of the collimator pairs used to produce the rectangular field. Equation (24), called the one-dimensional method, corrects for both of these effects and generally can predict the output factor within 1% (Mills ***et al.,*** 1985). Values of CF are zero at energies above 17 MeV and can be as large as 3% at the lowest energy, 6 MeV.

If the one-dimensional method is used, then a set of dose measurements must be taken in which Y is set at Y_0 and X

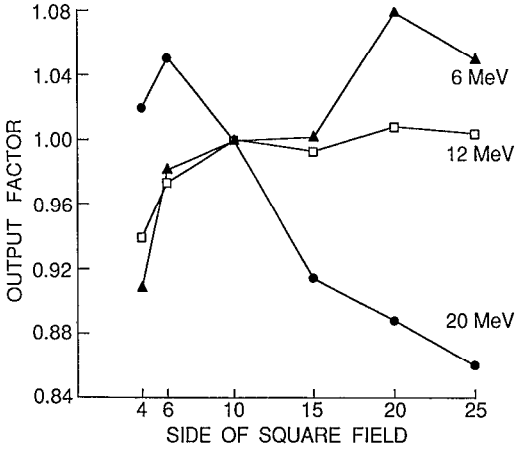

FIG. 20. Output factor as a function of the side of a square field for open applicator for 6-, 9-, and 12-MeV electrons. Redrawn from Purdy, 1982.

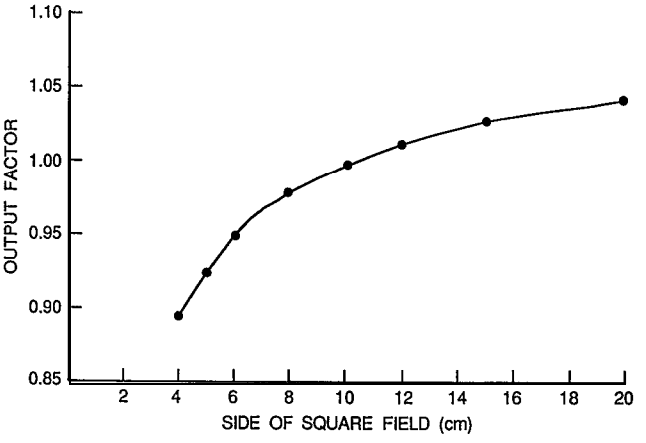

FIG. 21. Output factor for variable trimmer system as a function of the size of a square field for 9-MeV electrons. Redrawn from Mills et al., 1982.

varied and then X set at X_0 (typically 10 cm) and Y varied. If the data are taken with a cylindrical ion chamber, then its long axis should be parallel to the fixed length for each set of measurements so that no correction for stem effect is necessary.

C. Irregular fields

For most clinical situations, the treatment is designed to encompass the tumor with minimum normal tissues in the field. This often leads to irregular field shapes that may significantly differ from rectangles and circles. The calculation of output factors for arbitrarily shaped fields has not received adequate discussion in the literature. However, Clarkson scatter integration has been used (Dutreix and Briot, 1985), as well as a pencil-beam algorithm (Bruinvis, 1985) to calculate output factors. Computer summation methods for irregular electron fields are not universally available and may sometimes prove cumbersome in a clinical environment. However, for many treatment planning field designs it is not difficult to estimate an effective square field. The output may then be obtained by interpolation over the measured square, rectangular, and circular field data. This approach should prove effective for situations where side-scatter electron equilibrium has been established. Where this is not the case, particularly with small fields, special measurements should be made.

D. Tertiary collimation

Tertiary collimation is sometimes used to define the treatment field. This is usually accomplished by placing the beam-defining aperture at the patients surface (skin collimation) rather than at the level of the cones or trimmers. The output factor for this geometry is equivalent to that for the field size defined by the cone (open or with insert) or trimmer as long as the aperture dimensions allow for scatter equilibrium in the patient. This approximation can be applied so long as the depth of maximum dose for the field size defined by the open cone or its insert if present, is the same as that for the field size defined by the skin collimation. When this condition does not hold, individual measurements should be made.

VIII. ELECTRON SOURCE POSITION

The electron beam, exiting the vacuum window of a typical radiotherapy accelerator and bending magnet, travels along the collimator axis and is a pencil beam having a small but finite radial and angular spread. In passing through the accelerator end window, scattering foils, beam monitoring transmission ionization chambers, intervening air, and any other materials in the beam, the electrons undergo multiple Coulomb scattering. At a downstream plane (e.g., level of beam-defining collimator), the electron beam is now broad but appears to have emanated from an electron source. ICRU (1984) defines an effective ***extended electron source;*** this source, when placed in vacuum, would produce exactly the same distribution of the electron fluence in position and angle as the actual beam. Characterized by an effective position upstream of the plane, a mean-square radius, and a mean-square angular spread, the effective extended electron source is useful for radiation transport calculations.

For the purpose of clinical dosimetry and treatment planning it is desirable to represent the extended electron source by a point source in vacuum so that divergence correction formulae such as the inverse-square law can be applied. This point source is defined as the ***virtual point source*** (Pohlit, 1965). The virtual point source is defined for a plane perpendicular to the central axis of the electron beam, which should be at the standard patient SSD (normally at the isocenter). It is defined as the point closest to intersecting the back projection of the mean directions of motion of electrons passing through pixels within the defined plane (ICRU, 1984; Schroder-Babo, 1983). The virtual point source is typically upstream from, but close to the position of the effective extended electron source. The virtual point source is sometimes determined for the plane at the level of the final beam-defining collimator for the purpose of inputting into dose algorithms.

The decrease in output for extended treatment distances is partially due to the decrease caused by inverse square from the virtual source position. An additional decrease in output may arise because of a loss of side-scatter equilibrium (see Sec. VII), which is particularly significant for small field size and low energies.

Two methods of characterizing the decrease in output with increasing air gap are presented in this section. In the first method, the decrease is characterized by an inverse-square factor from an ***effective source.*** The term effective source should not be confused with the effective extended electron source defined earlier. Theoretically, the dose fall-off for extended treatment distances does not follow an inverse-square law; however, a position can be chosen to best fit measured data. This position is referred to as the effective source (Khan ***et*** al., 1978). In the second method the decrease in dose is characterized by the product of an inverse-square factor from the virtual source position and an air gap factor correcting for loss of side-scatter equilibrium and other scatter effects (e.g., collimator scatter). Either method is considered acceptable for calculating output at extended treatment distances, since parameters for each method are derived from the same set of measured data.

A. Virtual point source

A number of methods have been suggested for determination of the virtual source position. Pohlit (1965) used images of a grid of copper wires projected onto a photographic film. The virtual source was found by back projection of the wire images beyond their actual location. This method loses its usefulness when the wire images are not distinctly readable.

The multipinhole technique, developed by Schroder-Babo (1983), uses double conical holes in a metal plate. A film is placed about 15 cm behind the pinhole plate. The location of the virtual electron source can be determined from the projection of the pinholes on the film. This method is similar to Pohlit's method in that the copper wires are replaced by the pinholes in a metal plate.

Fehrentz ***et al.*** (1976)) Khan ***et al.*** (1978)) and Meyer ***et*** al. (1984) discussed the method in which off-axis beam pro-

files are measured at several distances from the end of the cone. The virtual source point is found by back projection of the 50% width of the beam profiles obtained at these locations. A large field (20×20cm2) should be used in these measurements to minimize the collimator influence and ensure side-scatter equilibrium.

The above methods give a virtual point source position that may be used to calculate the beam width defined by the width of the 50% decrement lines at various distances from the collimator by projection over the collimator edges (Meyer *et* al., 1984). However, its use to calculate the variation of dose rate with distance is limited (Jamshidi ***et al.,*** 1986). Except at high energies and large field sizes, where the influence of beam scattering on dose rate by the collimator and air is reduced, the use of the virtual SSD to predict dose variation with distance requires correction factors, in addition to the inverse-square law relationship, as a function of energy and field size.

B. Effective point source

For the purpose of correcting dose output for the air gap between the collimator and the patient, a method is recommended that simulates as closely as possible the clinical situation. In this method (Khan ***et al.,*** 1984), a series of output measurements are made in a phantom at the depth-of-dose maximum as a function of the air gap ***g*** between the cone end (or the plane perpendicular to the beam axis at the nominal SSD) and the phantom surface. If Q_0 is the ionization charge reading with zero gap and Q_0 is the reading with gap ***g,*** then, in accordance with the assumption of the inverse-square law,

$$\frac{Q_0}{Q_g} = \frac{(\mathrm{SSD}_{\mathrm{eff}} + d + g)^2}{(\mathrm{SSD}_{\mathrm{eff}} + d)^2}, \tag{23}$$

where $\mathrm{SSD}_{\mathrm{eff}}$ is the effective SSD and ***d*** is the depth of measurement. This can be written as

$$\left(\frac{Q_0}{Q_g}\right)^{1/2} = \frac{g}{(\mathrm{SSD}_{\mathrm{eff}} + d)} + 1. \tag{24}$$

By plotting $[Q_0/Q_g]^{1/2}$ as a function of g (Fig. 22), a straight line is obtained having slope $1/(\mathrm{SSD}_{\mathrm{eff}} + d)$. The effective SSD is then equal to

$$\mathrm{SSD}_{\mathrm{eff}} = (1/\mathrm{slope}) - d. \tag{25}$$

Depending upon beam energy, type of collimator, and field size, the plot of $[Q_0/Q_g]^{1/2}$ versus g may gradually deviate from a straight line beyond a certain air gap [Figs. 23(a), (b), (c)]. For small field sizes and low energies, the effective SSD and inverse-square law method of correcting output is valid only for a limited range of air gaps, up to about 15 cm in most cases. For larger SSDs beyond the range of inverse-square law applicability, a new output calibration should be obtained. Alternatively, $[Q_0/Q_g]^{1/2}$ versus g plots may be used directly to correct the output if data extend to large SSDs.

Although the effective SSD is obtained by making output measurements at the depth of maximum dose, its value does not change significantly with the depth of measurement (Khan ***et al.,*** 1978). Thus the entire depth-dose curve can be corrected by the same effective SSD.

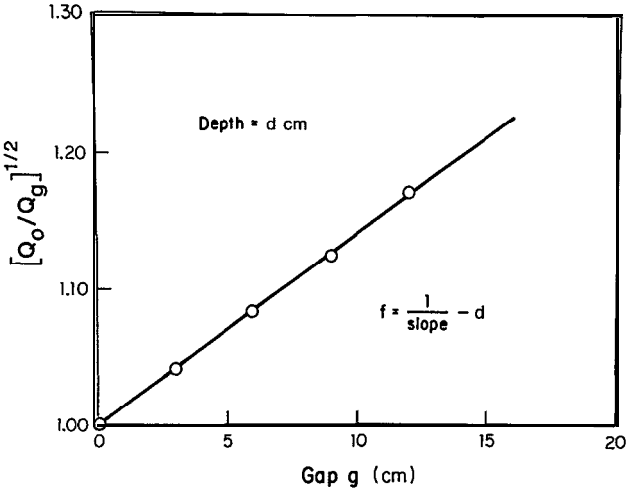

FIG. 22. Determination of effective source-to-surface end distance (f). The parameters Q_0, Q_g, g, and d are explained in the text. Plotted data correspond to a 10-MeV electron beam with a 10-cm-diam cone, and $d = 1.43$ cm in polystyrene. [From Khan *et al.* (1978).]

C. Corrections for air gaps or extended SSD

Usually, the final collimation device of an electron beam is either a treatment cone, a fixed collimator, or a variable collimator, which defines the treatment field at some fixed distance from its end. Ideally, the patient's skin surface would lie at that distance under standard treatment conditions. However, frequently it becomes necessary to treat with nonstandard treatment distances because of either an anatomical restriction, such as a shoulder in neck treatment, or an irregular skin surface. In addition, extended treatment distances can be used to obtain larger field sizes or increased penumbra.

The effect of a nonstandard SSD on machine output and dose distributions must be assessed in order to assure proper patient treatment. The majority of nonstandard SSD treatments are at an extended SSD, and as a general rule one should avoid such treatments unless absolutely necessary. As discussed below, extending the SSD typically produces a significant change in output, a minimal change in depth dose, and a significant increase in the beam penumbra. If the beam is also entering obliquely to the patient surface, then there can be further alteration of the depth dose (see Sec. X). All of these effects depend strongly on machine, energy, field size, and treatment distance so that it is not recommended to simply extrapolate from data measured under different conditions. Detailed calculations or measurements are required for individual machines and circumstances.

1. Correction of output

The relationship between maximum dose at the nominal (calibration) SSD and the maximum dose at the extended SSD is called the output correction. Two methods of output correction are typically used, namely, the effective SSD method and the virtual SSD method.

In the effective SSD method, the dose D'_{max}, at an extended

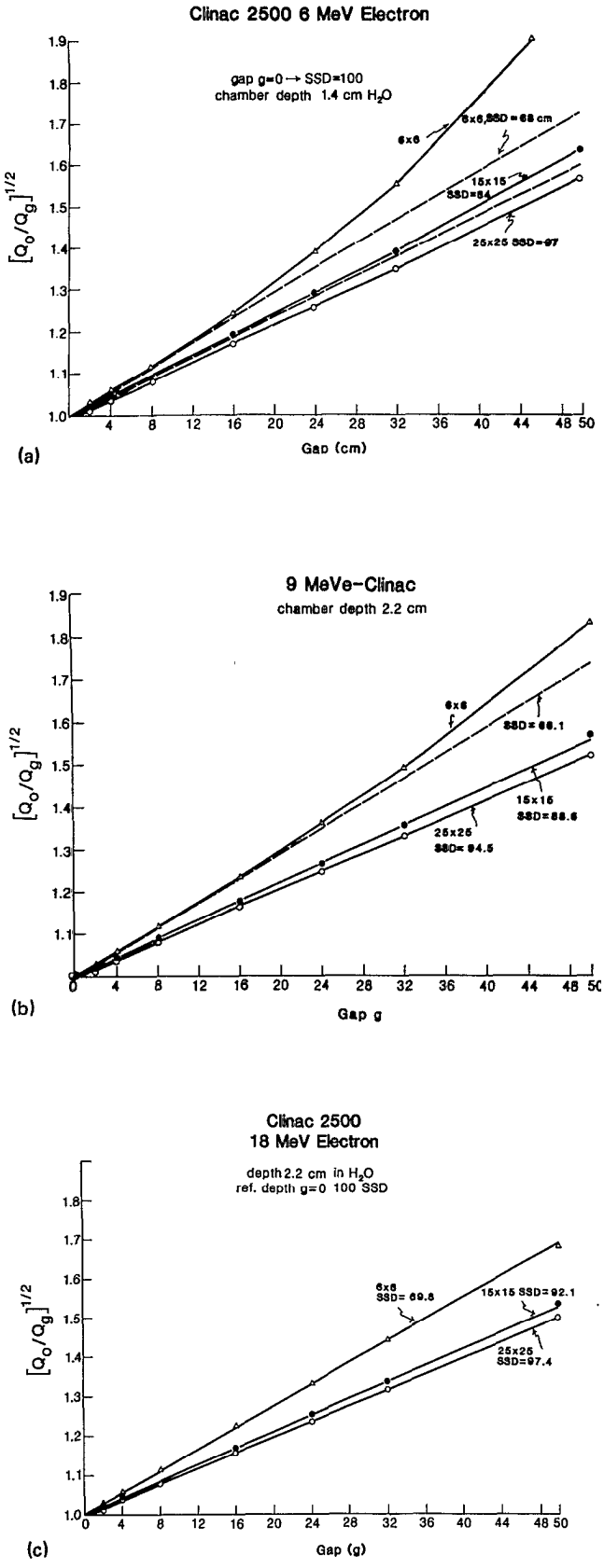

FIG. 23. (a) Determination of effective SSD using method described in text for 6-MeV electrons for different field sizes and nominal SSDs. (b) Determination of effective SSD using method described in text for 9-MeV electrons for different field sizes and nominal SSDs. (c) Determination of effective SSD using method described in text for 19-MeV electrons for different field sizes and nominal SSDs. [From Deibel and Khan (1984).]

SSD' is related to the dose D_{max} at the nominal SSD by the following inverse-square law relationship:

$$D'_{\max} = D_{\max} \frac{(\mathrm{SSD}_{\mathrm{eff}} + d_{\max})^2}{(\mathrm{SSD}_{\mathrm{eff}} + g + d_{\max})^2}, \tag{26}$$

where $\mathrm{SSD}_{\mathrm{eff}}$ is the effective SSD for calibration for the given collimator field size and energy, g equals the difference between SSD' and SSD, and d_{max} is the depth of maximum dose on central axis. As stated earlier the inverse square law relationship may not be exactly followed for the treatment conditions involving low electron energies and large air gaps. In those cases, either the $[Q_0/Q_g]^{1/2}$ versus g data measured for various field sizes, electron energies, and air gaps may be used directly or a new calibration may be performed for the given treatment conditions.

In the virtual SSD method, the dose at the extended treatment distance is given by

$$D'_{\max} = D_{\max} \frac{(\mathrm{SSD}_{\mathrm{vir}} + d_{\max})^2}{(\mathrm{SSD}_{\mathrm{vir}} + g + d_{\max})^2} f_{\mathrm{air}}, \tag{27}$$

where $\mathrm{SSD}_{\mathrm{vir}}$ is the virtual SSD for calibration and f_{air} is the air gap correction factor. If the treatment field is rectangular, then from the work of Mills *et al.* (1982) it can be shown that a good estimate off,,, is

$$f_{\mathrm{air}}(X,Y,g) = [f_{\mathrm{air}}(X,X,g) \times f_{\mathrm{air}}(Y,Y,g)]^{1/2}. \tag{28}$$

Meyer *et al.* (1984) have reported values of f_{air} for the Siemens Mevatron 77. The variation of f_{air} versus g with field size at 7 MeV and the variation with energy for a 6 x 6 cm^2 field size are shown in Fig. 24(a) and (b), respectively.

This method represents an alternative approach to the effective SSD method, using the same set of measured data. Both methods are consistent with the suggestion of Thomadsen *et al.* (1981) to measure any output at an extended distance, as they both provide a methodology for storing and using the data.

2. Correction of dose distribution

The use of an extended treatment distance has only minimal effect on the central-axis depth dose and the off-axis ratios. Under the treatment conditions in which the dose rate changes with the effective SSD in accordance with the inverse-square law, the depth-dose distribution can be calculated according to

$$\%D(d,\mathrm{SSD},g) = \%D(d,\mathrm{SSD},0) \times \frac{[(\mathrm{SSD}_{\mathrm{eff}} + d)/(\mathrm{SSD}_{\mathrm{eff}} + g + d)]^2}{[(\mathrm{SSD}_{\mathrm{eff}} + d_{\max})/(\mathrm{SSD}_{\mathrm{eff}} + g + d_{\max})]^2}, \tag{29}$$

where the depth dose equals 100% at d_{max} for both standard and extended SSD. For typical values of $\mathrm{SSD}_{\mathrm{eff}}$, g, d, and d_{max} ($\mathrm{SSD}_{\mathrm{eff}}$ = 100 cm, d_{max} = 2 cm, g < 10 cm, d < 15 cm) this correction will have an insignificant effect (< 1 mm) on the shape of the depth-dose curve (< 1 mm shift on descending portion) so that the use of the standard depth-dose curve should be an acceptable approximation at extended distances.

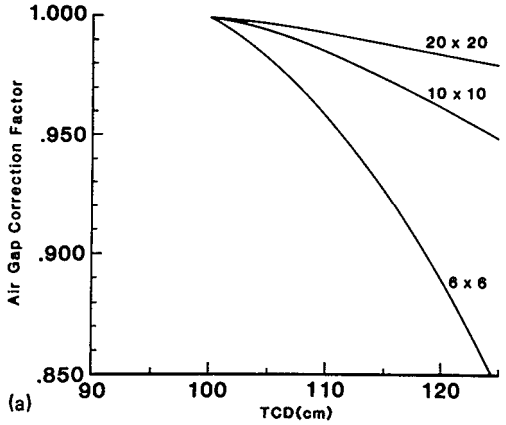

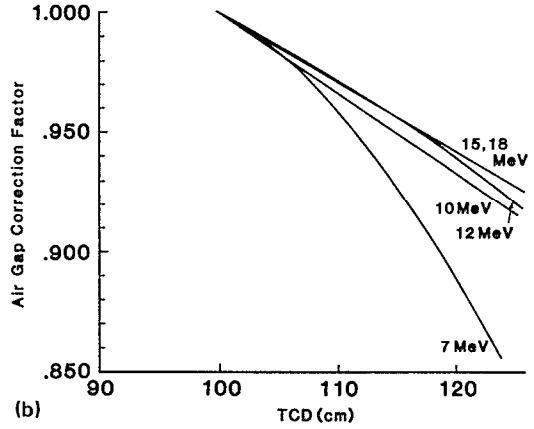

FIG. 24. (a) Air gap correction factor for 7-MeV electrons as a function of nominal SSD for varying square fields. (b) Air gap correction factor for a 6x6 cm^2 field as a function of nominal SSD for varying electron beam energy. [From Meyer *et al.* (1984).]

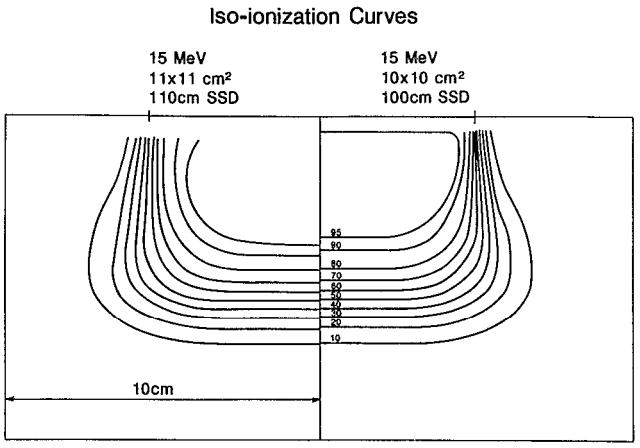

FIG. 25. Comparison of iso-ionization curves measured for nominal SSD as opposed to extended SSD conditions. [From Hogstrom *et al.* (1984).]

When electrons scattered from the collimator are sometimes added to the beam for field uniformity, extended treatment distances can affect field flatness and penumbra width. As discussed by Hogstrom *et al.* (1981), and Khan *et al.* (1978), the penumbra width (80%-20%) at shallow depths increases with distance from the collimator, particularly at the lower electron energies (< 10 MeV). This effect is illustrated in Fig. 25, which compares isodose distributions at the nominal SSD and an extended SSD.

The increase of penumbra width with SSD makes manual methods of generating dose distributions at extended distances unreliable, particularly for cases where the dose distribution at the beam's edge is critical. Various computer methods have been proposed for use with electron-beam dose calculations. This section will not undertake the task of performing a comprehensive review of such algorithms but will illustrate examples of algorithms that make or do not make an attempt to properly account for extended SSD distributions. It is the responsibility of the individual to determine the accuracy of his or her electron-beam treatment planning computer algorithm.

The early computer algorithms for electrons were based on interpolation from measured data. The variable fan line-depth line interpolation algorithm by Khan and Lee (1979) addressed the problem of air gaps but made only an inverse-square correction at each point to the dose, extracted from a set of data measured at the nominal SSD. The resulting curves do well on the central axis and within the central region of the beam but fail to predict accurately the broader penumbra at the extended SSD as was shown by comparison of measurement and calculation (Khan and Lee, 1979). The Memorial electron beam Absorption Equivalent Thickness Factor (AET) algorithm described by Holt *et al.* (1978) also interpolates from measured data, but interpolates between data measured at two SSDs so that the effects of an extended SSD are taken into account. The newer class of computer algorithms for electrons are the pencil-beam summation models, which are usually also based on measured data. The ability of these algorithms to accurately calculate dose distributions at extended SSD (Hogstrom *et al.*, 1987) must be evaluated on an individual basis.

D. Clinical considerations for extended SSD

It is the recommendation of this task group that the following considerations be made for treatment at extended SSD:

(i) All extended SSD treatments should be considered as potentially delivering a dose and/or dose distribution to the patient which is significantly different from that which the radiation therapist has intended, and as such, dosimetry personnel should have both well-defined guidelines for its use and methods for indicating when existing data can be used and when individual dose measurements are required.

(ii) Dosimetry differences due to extended SSD typically increase with decreasing energy, decreasing field size, and increasing SSD.

(iii) It is possible to restore the penumbra when treating at extended SSD by placing collimation on the skin surface. In doing so, the inside edge of the skin collimator should lie well inside the penumbra cast by the normal collimating device. If skin collimation is used, the field size defined by the normal treatment collimator is the primary influence on the

output, whereas the field size defined by the skin collimator is the primary influence on the depth-dose distribution. Individual dose measurements are recommended in such cases.

(iv) The increase in penumbra at extended SSD may be useful for abutting radiation fields. It is necessary that an accurate dose distribution be used for determining the overlapped distribution, but only a few of the current dose algorithms can calculate the distribution properly. Film is a useful method of verifying the dose distribution in the junction region of abutting fields.

(v) Premeasured tables or graphs may be used to compute output at the extended SSD. If there is any question about the applicability of the inverse-square law, then measurement simulating patient conditions is recommended.

(vi) These considerations are intended for extended SSD approximately 15 cm or less from the standard SSD. For a discussion of total skin irradiation at extremely extended SSD, the reader is referred to AAPM Report No. 23 (1988).

IX. FIELD SHAPING AND SHIELDING

Electron-beam fields can be shaped with lead strips or cutouts, placed either directly on the skin surface or at the end of the collimator. The thickness of lead required depends on the beam energy and the desired transmission through the shield. The transmitted dose varies with incident electron energy, primary bremsstrahlung dose, field size, and the gap between the patient and the collimator. For a particular machine, the maximum transmission typically occurs at the highest energy and when the collimation is in direct contact with the skin.

In most cases of external shielding, a transmitted dose value of $\leq 10\%$ is considered acceptable. For internal shielding, however, the allowed transmission depends on the space available for the shielding. In the case of eye shields, the lead thickness is determined by what can be accommodated comfortably under the lid, and the transmitted dose to the lens is reduced to within acceptable limits (Asbell *et al.*, 1980).

A. Shielding thickness

The measurement of the transmission curves through shielding material for various electron energies can be made with a plane-parallel ion chamber in a phantom such as polystyrene. Transmission curves may be obtained by plotting ionization as a function of shield thickness. The maximum transmitted dose occurs at a point close to the skin surface. Thus it is important that the distance between the chamber and the lead is minimal (less than 0.5 cm) (Khan *et al.*, 1981).

It has been shown that the shielding measurements made with broad beams give an upper limit to the shielding requirements for all field sizes (Giarratano *et al.*, 1975; Purdy *et al.*, 1980). For internal shielding, however, where minimum thickness shields may be required, transmission measurements should be made specifically for the given field size and the depth of the structure to be shielded.

Figure 26 is a plot of minimum lead thicknesss required to stop all of the electrons (transmitted dose only due to bremsstrahlung) as a function of the most probably energy incident on the lead and shows a linear relationship. As a useful rule of thumb, the thickness of lead in millimeters required for shielding is approximately given by the energy in MeV divided by two. If Lipowitz alloy (Cerrobend) is used, its thickness should be 1.2 times that required using lead.

B. Internal shielding

Internal shielding is useful in some situations such as the treatment of lip, buccal mucosa, and eyelid lesions. Internal

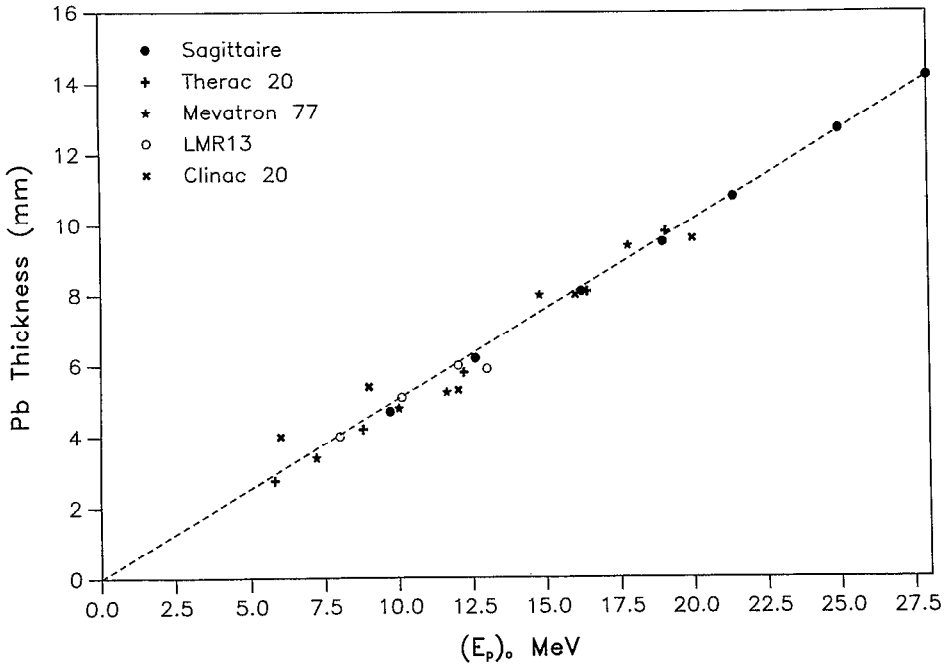

FIG. 26. A linear regression plot of published data for lead thickness required to stop primary electrons as a function of electron energy; slope = 0.50-mm Pb/MeV; standard error of estimate = 0.36-mm Pb. [LMR 13 dam from Khan *et al.* (1976), Clinac 20 data from Purdy *et al.* (1980) and the rest of the data from K. R. Hogstrom (personal communication).]

shielding can be accomplished by placing a lead shield beyond the target volume to protect the underlying normal structures. It must be noted that the electron backscatter produces significantly large dose enhancement near the tissue-lead interface. This problem has been studied by various investigators (Khan *et al.*, 1976; Saunders and Peters, 1974; Nusslin, 1974; Gagnon and Cundiff, 1980; Okumura *et al.*, 1971; and Klevenhagen *et* al., 1982). The enhancement in dose at the tissue-metal interface is dependent on beam energy at the interface and the atomic number of the metal. In the case of tissue-lead interface, the following equation by Klevenhagen *et al.* (1982) may be used to estimate electron backscatter factor (EBF) :

$$\mathrm{EBF} = 1 + 0.735 \exp(-0.052\,\overline{E}_d), \qquad (30)$$

where $\overline{E}_d$ is the average energy of the electrons incident at the interface. Figure 27 shows the variation of EBF with atomic number of the scattering material for a wide range of energies.

Dose enhancement due to electron backscatter can either be taken into account in treatment planning (Okumura *et* al., 1971) or be minimized by interposing a low atomic number material between the lead and overlying tissue. Since the backscattered electrons have a significant range, the thickness of the low atomic number shield should be sufficient to absorb the backscattered electrons. Lambert and Klevenhagen (1982) have determined transmission curves through polystyrene for the backscattered electrons (Fig. 28) that may be used for designing the shield. Internal shielding is usually custom-designed and dosimetrically checked using a plane-parallel chamber or film imbedded in a polystyrene phantom.

X. EFFECTS OF OBLIQUE INCIDENCE AND HETEROGENEITIES

Basic electron-beam data are applicable to beams normally incident on water or water equivalent, homogeneous media with flat surfaces. In clinical applications, however, situations arise where the patient's surface contour is curved and when there are significant tissue heterogeneities present. In these situations, the additional factors that influence the dose distribution within a patient are

(i) changes in electron scattering, (ii) changes in electron beam penetration, and (iii) interface effects.

This section discusses the effects of curved surfaces and tissue heterogeneities on dose distribution. Methods to take into account the perturbation in dose due to oblique incidence of the beam on skin surfaces and tissue heterogeneities are described.

For a review of the effects of tissue heterogeneities on electron dose distributions, see Hogstrom (1983).

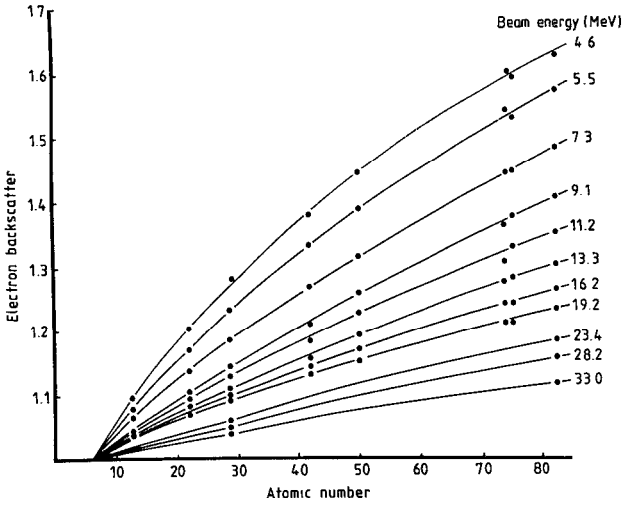

FIG. 27. Variation of electron backscatter with atomic number Z of scattering material. Curves for different beam energies at the scatter surface are shown. [From Klevenhagen *et al.* (1982).]

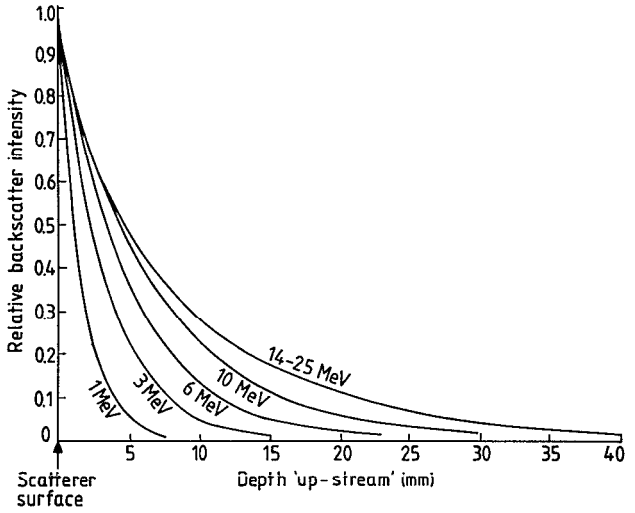

FIG. 28. Penetration of electrons backscattered from lead into polystyrene in the "up-stream" direction of the primary beam. [From Lambert and Klevenhagen (1982).]

A. Oblique incidence

In situations where the beam obliquity is small (angle of incidence smaller than 30°), the effect of obliquity in the central portion of the field is to shift the isodose curves parallel to the skin surface; therefore, the depth dose along the central axis is approximately the same as that for normal incidence (Okumura, 1972; Almond, 1976; ICRU, 1984). When beam obliquity is large (angle of incidence greater than 30°), the effects of laterally scattered electrons become important and give rise to significant changes in dose distribution. Changes in central-axis dose include (i) increase in dose near the depth-of-dose maximum, (ii) shift of the therapeutic depth towards the surface, and (iii) increase in dose at oblique depths near the practical range.

These effects are illustrated in Fig. 29 from Ekstrand and Dixon (1982). For example, for 9-MeV electrons incident at an angle of 45°, (1) the increase in dose near the depth of maximum dose is approximately 10%, (2) the R_{90} is shifted 8 mm toward the surface, and (3) the dose near the practical range is approximately 20%. As a clinical example, the dose distribution for a 10-MeV electron beam incident on a curved surface with small radius of curvature (calf of a pa-

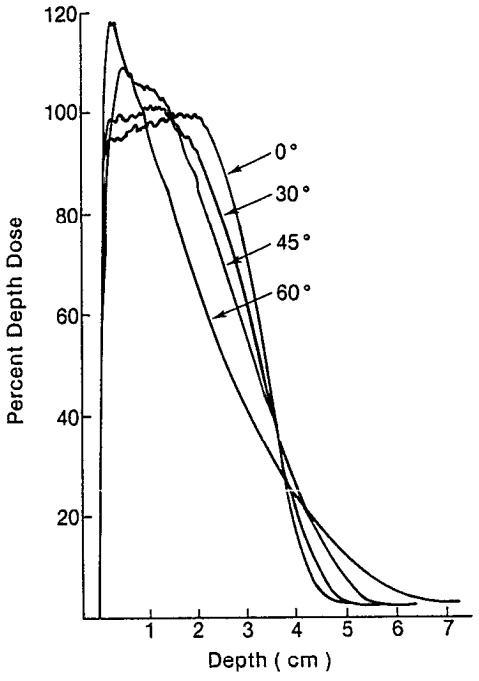

FIG. 29. Variation of central-axis depth dose with obliquity for 9-MeV electron beams. (Redrawn from Ekstrand and Dixon, 1982.)

tient's leg) has been reported by McKenzie (1979) and is shown in Fig. 30. Hot spots on the lateral borders of the calf are produced where the dose is approximately 10% higher. Changes in the penumbral region include (a) widening of the penumbral width on the side of the field farthest from the collimator and (b) narrowing of the penumbral width on the side of the field nearest the collimator.

Khan *et al.* (1985) have shown that the dose for an obliquely incident beam can be calculated from the central-axis depth dose for a normally incident beam by using the inverse-square law and obliquity factors. The obliquity factor accounts for the change in dose due to the oblique incidence of the beam. This factor, defined by Eq. (31), depends on the angle of incidence, depth, and beam energy. For an obliquely incident beam, the parameter required for calculation of dose at a point off the central axis but in the central portion of the beam and away from the penumbra is shown by the diagrams in Fig. 31. If $D(d, \mathrm{SSD}_{vir})$ is the dose along the central axis at depth d for the virtual source-to-skin distance SSD_{vir} the dose, $D(d, \mathrm{SSD}_{vir}+g)$, at depth d with an air gap of g is given by

$$D(d,\mathrm{SSD}_{vir}+g)=D(d,\mathrm{SSD}_{vir})\frac{(\mathrm{SSD}_{vir}+d)^2}{(\mathrm{SSD}_{vir}+d+g)^2}\times f_{air}f_{ob}(\theta,d). \quad (31)$$

In the above equation, f_{air} is the air gap correction factor defined in Sec. VIII C1, and $f_{ob}(q, d)$ is the obliquity factor. Equation (3 1) is strictly applicable only to flat surfaces but can be applied to patient surfaces that are nearly flat. For various angles of incidence, data for obliquity factors published by Khan *et al.* (1985) for a particular machine are found in Table XII. In principle these data should be applicable to other radiotherapy machines. It should be noted that for curved surfaces, such as the chest wall, the dose near the surface may be either hot or cold, depending on the relative values of the inverse-square term, and the obliquity factor.

Sharp surface irregularities where the electron beam may be incident tangentially give rise to a complex dose distribution with localized overdose (hot spot) and underdose (cold spot). An example is demonstrated in Fig. 32 where the electron beam is incident on a phantom with sharp boundary between air and water. The scattering of electrons from the outward projected water column gives rise to hot spots laterally. This situation is similar to that encountered in the treatment of nasal cavity by an anterior electron beam. Tapered bolus around the nose may be used to smooth out the surface irregularity and eliminate the hot spot.

B. Tissue heterogeneities

The problem of tissue heterogeneities is one of the major challenges of electron-beam dosimetry. Several investigators have reported the effect of heterogeneities on dose distribu-

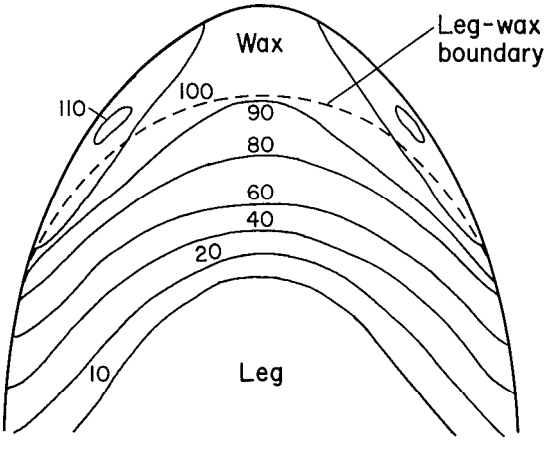

FIG. 30. Measured dose distribution in a phantom irradiated with a single incident beam of 10-MeV electrons. (Redrawn from McKenzie, 1979.)

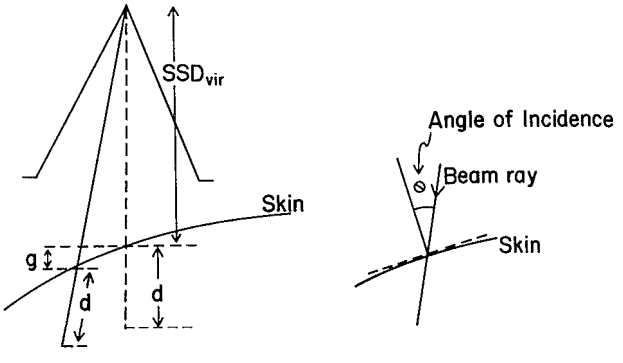

FIG. 31. Oblique incidence of a beam with an air gap.

TABLE XII. Obliquity factors for electron beams measured by Khan *et al.* (1985) on a Varian Clinac 2500 linear accelerator. Z is the depth measured along the line joining the point of measurement to the virtual electron source.

	E_0 (MeV)					
Z/R_p	22	18	15	12	9	6
(a) $\theta = 30°$						
0.0	1.00	0.98	0.98	1.00	0.94	1.01
0.1	1.00	1.00	1.00	1.00	1.00	1.08
0.2	1.00	1.00	1.01	1.02	1.05	1.11
0.3	1.01	1.00	1.02	1.03	1.05	1.06
0.4	1.01	1.01	1.02	1.00	1.00	0.96
0.5	1.00	1.00	0.98	0.96	0.92	0.86
0.6	0.95	0.94	0.92	0.90	0.86	0.79
0.7	0.92	0.90	0.87	0.86	0.86	0.83
0.8	0.93	0.85	0.82	0.90	1.00	0.96
0.9	1.09	1.00	1.20	1.11	1.44	1.00
1.0	1.42	1.54	1.50	1.50	1.30	1.00
(b) $\theta = 45°$						
0.0	1.03	1.02	1.03	1.05	0.98	1.14
0.1	1.03	1.04	1.04	1.06	1.10	1.14
0.2	1.05	1.06	1.07	1.11	1.12	1.12
0.3	1.06	1.07	1.09	1.09	1.05	1.07
0.4	1.04	1.04	1.04	1.01	0.93	0.92
0.5	1.00	0.99	0.92	0.92	0.80	0.77
0.6	0.93	0.90	0.86	0.82	0.70	0.69
0.7	0.84	0.84	0.82	0.77	0.70	0.76
0.8	0.87	0.83	0.85	0.86	0.83	1.10
0.9	1.30	1.00	1.43	1.20	1.40	1.46
1.0	2.17	2.31	2.19	2.50	2.00	2.14
(c) $\theta = 60°$						
0.0	1.06	1.06	1.10	1.14	1.14	1.30
0.1	1.10	1.12	1.17	1.20	1.23	1.21
0.2	1.12	1.14	1.15	1.16	1.17	1.08
0.3	1.07	1.07	1.07	1.02	0.98	0.90
0.4	1.00	0.96	0.93	0.86	0.79	0.70
0.5	0.87	0.84	0.79	0.74	0.67	0.56
0.6	0.75	0.74	0.69	0.63	0.58	0.51
0.7	0.70	0.68	0.67	0.62	0.57	0.56
0.8	0.75	0.71	0.67	0.74	0.77	0.87
0.9	1.21	1.00	1.29	1.14	1.60	1.40
1.0	2.31	2.46	2.75	3.0	3.2	2.45

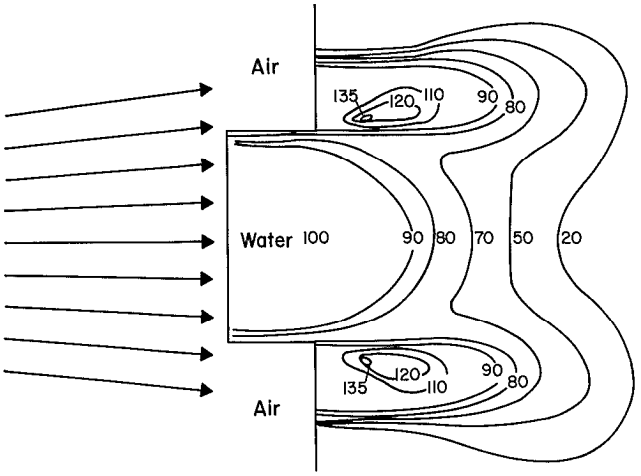

FIG. 32. Electron beam impinging on a water surface tangentially gives rise to hot spot laterally. (Redrawn from ICRU, 1974.) (Dutreix, 1970.)

tion for electron beams (Laughlin *et al.*, 1965; Boone *et al.*, 1967; Almond *et al.*, 1967; Brenner *et al.*, 1969; Pohlit, 1969). These studies showed that the magnitude of the dose perturbation depends on the shape, size, electron density (number of electrons/cm^3), and the effective atomic number of the heterogeneity.

Computed tomography gives accurate localization of heterogeneities and can be used to determine their electron density (Parker *et al.*, 1979; Hogstrom *et al.*, 1981). In spite of all the significant advances that have been made in electron-beam dosimetry in solving the heterogeneity problem, only modest progress has been made in their clinical implementation. In many instances the classical empirical methods such as CET (coefficient of equivalent thickness) or AET Factor are still used. A current review of these methods and their limitations are discussed in ICRU (1984), and only a brief discussion is presented here.

For relatively large heterogeneities that can be approximated as uniform slabs, a simple but not always accurate method is the CET method. CET is defined (for a parallel beam) as the ratio of the thickness of water to that of the inhomogeneity that produces the same transmission of absorbed dose rate. The CET for a given material of atomic number Z and density r not very different from water is approximately equal to the ratio of total linear stopping power of the material relative to water. When the stopping power for the material is not known, the CET value may be estimated from the ratio of the electron density (electron/cm") relative to that of water. The dose at a point beyond the inhomogeneity is determined by calculating the effective depth d_{eff}, along the ray joining the point and the virtual source of the electrons:

$$d_{eff} = d - t\,(1 - \mathrm{CET}), \tag{32}$$

where d is the actual depth of the point and t is the thickness of the inhomogeneity. The percent depth dose for the point is read from the depth-dose data in water for the electron-beam energy under consideration at the effective depth d_{eff} and then corrected for the inverse-square law. CET, in general, varies with depth in the tissue and with beam energy (Almond *et al.*, 1967; Boone *et al.*, 1967). For lung tissue, the CET decreases with increasing depth and increases with increasing electron energy. In the case of bone, the CET depends on its electron density and the distance from the bone-tissue interface. Ignoring the interface effects, the CET for a compact bone (e.g., mandible) is approximately 1.65 (equal to its relative electron density), and for a spongy bone, such as sternum, CET is close to unity.

An increase in dose within bone and in soft tissue immediately below the bone has been reported (ICRU, 1984; Prasad *et al.*, 1984). Measurements by Prasad *et al.* (1984) using TLD and film suggest a dose enhancement in compact bone. Because of the difficulty inherent in interface dosimetry measurements and scarcity of data, the magnitude of dose enhancement in bone remains uncertain. Also, lateral to the edge of the bone-water interface, hot and cold spots are produced (ICRU, 1984; Pohlit, 1969). The magnitude of these effects depends on the electron density and shape and thickness of bone.

Several investigators have studied the effect of air heterogeneity on dose (Brenner *et al.*, 1969; ICRU, 1984; Pohlit, 1969). For example, calculations by Hogstrom (1983) illustrate in Fig. 33 that the dose behind an air cavity, having a 2X2 cm^2 cross-sectional area, increases by 10%-30% depending on the depth of interest for a 17-MeV electron beam.

Dose to lung tissue is of considerable interest in the treatment of chest wall and mediastinum. Studies with CT have revealed that the average density of lung tissue relative to water is 0.25 (Rosenblum *et al.*, 1980; Van Dyk *et al.*, 1980). This implies that the range of electrons in lung tissue will be considerably larger than in soft tissue. Corrections for lung tissue using CET methods are based on measurements made in cork (Laughlin, 1965; Boone *et al.*, 1967; Almond, 1976). These methods suggest that CET for lung depends on the density of lung, the depth, the field size, and the energy of the beam. Dahler *et al.* (1969) have, however, suggested that in actual practice it is adequate to use an average values of CET. These authors have proposed that an average CET can often be taken as 1.3 times the relative density of lung. Recent measurements by Prasad *et al.* (1983) in Rando phantom suggest that calculations based on water equivalent depth where CET is assumed to equal the relative density of lung gives better agreement than the average CET.

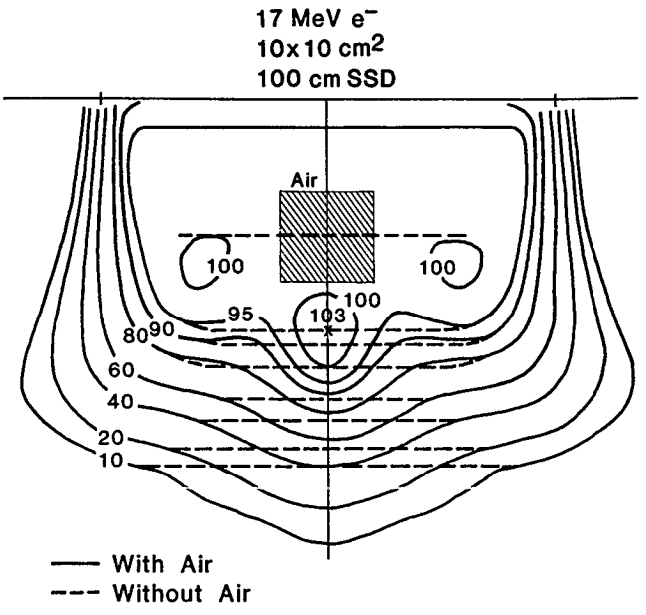

FIG. 33. Perturbation of the dose distribution caused by an air cavity of 2 X 2 cm' in cross section. Redrawn fram Hogstrom (1983).

One readily appreciates that a determination of dose distribution perturbed by heterogeneities of different shapes and densities is complex, and it is no surprise that the CET type methods fall short. Algorithms based on a pencil-beam multiple Coulomb scattering model are now being developed to compute more reliable dose distributions. For additional information refer to the review articles by Hogstrom (1987) and Brahme (1985).

XI. GUIDELINES FOR DOSE SPECIFICATION FOR ELECTRON BEAMS

The dose distribution, whether it be produced by photon beam irradiation or by electron beam, is generally not uniform within the target volume. However, for the purpose of specifying a dose prescription, a nominal dose, called the target dose (TD), should be defined in accordance with the ICRU (1978). As a general rule, the TD cannot be specified by the maximum and minimum dose within the target volume since they are not always representative of the overall dose distribution. Although local tumor control depends on the minimum dose to the tumor volume, the use of the minimum TD alone is not recommended since difficulties in determining the extent of the tumor volume may reduce its clinical significance and further may lead to ambiguity in its definition.

The dose selected for reporting should be chosen to be representative of the dose distribution within the target vol-

ume and its calculation should, if possible, not require special computation facilities. It should be understood that the target dose as specified represents a minimum requirement for reporting and often carries limited clinical information. Finally, it should be understood that the specification of target dose for reporting depends on the treatment technique, and its significance can only be interpreted when adequate information describing the radiation technique has been given.

The recommendations of this task group regarding dose specification follow very closely those put forth by the ICRU (1978) and those adopted by the Radiation Therapy Oncology Cooperative Studies Group (RTOG) and are as follows:

(i) The electron-beam radiation quality should be specified by the energy (MeV) and the type of radiation machine.

(ii) The nominal source-to-surface distance (SSD), the applicator (cone) size, and the treatment field size should be specified.

(iii) Any other beam modification devices such as energy moderators, patient bolus, etc. should also be specified.

(iv) If tissue heterogeneity corrections are made it should be so stated.

(v) The target dose should be specified at a point at the depth of maximum dose on the central axis in a water phantom for the field size and SSD used to treat the patient.

(vi) The dose prescription point should not be in a high-dose gradient area, for example, near the edge of the field, and generally, not in a blocked area.

(vii) The energy and field size should be chosen and so specified such that the target volume is encompassed within 90% (or any other appropriate minimum dose) of the prescribed dose.

(viii) The allowed variation of the dose across the target volume should be described relative to the target dose.

ACKNOWLEDGMENTS

The Task Group acknowledges the assistance of Dr. William Hanson who provided the travel funds from the Radiological Physics Center. (NCI Grant No. CA 10953) and made arrangements for two Task Group meetings. We appreciate members of the Radiation Therapy Committee, the Science Council and the editorial staff of Medical Physics for their review and comments. We gratefully acknowledge the assistance of Martha Hill, Cheryl Zmaila and Sally Humphreys for their superb job of typing and keeping the manuscript organized through its endless revisions.

LIST OF SYMBOLS

C_1	constant used in energy determination
C_2	constant used in energy determination
C_3	constant used in energy determination
C_4	constant used in energy determination
C_o	cone size for reference field
C_s	cone size
CET	coefficient of equivalent thickness
CF	collimator factor
d	depth in medium
d_{center}	depth of the center of ion chamber
d_{eff}	effective depth
d_{front}	depth of the front of proximal side of a plane-parallel chamber
$d_{\max}$	depth-of-dose maximum
$d_{\max,0}$	depth of dose maximum for reference field
d_{med}	depth in medium
d_{water}	depth in water
D/U	dose per monitor unit
D_{med}	dose to medium
D_{water}	dose to water
$D_{\max}$	dose at depth-of-dose maximum
$D'_{\max}$	dose at depth-of-dose maximum at extended SSD
$\overline{E}_d$	mean electron energy at depth d
$\overline{E}_0$	mean electron energy at surface
E_p	mean probable energy
$E_{p,0}$	most probable energy at surface
EBF	electron backscatter factor
F	field size
F_0	reference field size
f_{air}	correction factor for air gap
f_{ob}	correction factor for obliquity
$f_{\text{linearity}}$	correction factor for TLD nonlinearity
$F(\text{OD})$	correction factor for film response
g	air gap
G_0	dose gradient
I_0	reference insert size
I_s	insert size
$\overline{L}/\rho$	mean restricted collision mass stopping power
K	depth-dependent constant for dose determination using ionization chamber
OD	optical density
OD_{net}	net optical density
OF	output factor
P_{ion}	ion recombination correction factor
P_{repl}	replacement correction factor
$\%D$	percent dose
$\%D_s$	percent dose on surface
$\%D_x$	percent dose due to photons
$[\phi]^{\text{water}}_{\text{med}}$	ratio of fluence in water to that in medium
Q	ionization charge
Q_+	ionization charge collected for + voltage
Q_-	ionization charge collected for - voltage
Q_{corr}	corrected ionization charge
Q_0	ionization charge with no air gap
Q_g	ionization charge with air gap
r	radius of ionization chamber's collecting volume
R_{50}	depth of 50% dose or ionization
R_{80}	depth of 80% dose or ionization
R_{85}	depth of 85% dose or ionization
R_{90}	depth of 90% dose or ionization
R_{100}	depth of 100% dose or ionization
R_p	practical range
R_q	depth of the intersection point
R_t	therapeutic range
ρ_{eff}	effective density
$(\overline{S}/\rho)_{\text{coll}}$	mean unrestricted collision mass stopping power

S	TLD sensitivity, dose per unit TL response
S_{cal}	S for a calibration dose
SSD	nominal source-to-surface distance
SSD_{eff}	effective SSD
SSD_{vir}	virtual SSD
TL	thermoluminescent dosimeter response
$TL_{background}$	thermoluminescent dosimeter background
t	thickness of tissue inhomogeneity
U	monitor unit
X	width of a rectangular field
X_0	width of a reference field
Y	length of a rectangular field
Y_0	length of a reference field

AAPM (1983). American Association of Physicists in Medicine, RTC Task Group 21, "A protocol for the determination of absorbed dose from high-energy photon and electron beams," Med. Phys. 10, 741-771.

AAPM (1988). American Association of Physicists in Medicine, *Total Skin Electron Therapy: Technique and Dosimetry,* AAPM Report No. 23 (American Institute of Physics, New York).

Almond, P. R. (1981). 'Characteristics of current medical electron accelerator beams," p. *43-53* in *Proceedings of the Symposium on Electron Beam Therapy,* Chu, F. C. H. and Laughlin, J. S. Eds. (Memorial Sloan Kettering Cancer Center, New York).

Almond, P. R. (1976). "Radiation Physics of Electron Beams," in *Clinical Applications of the Electron Beam,* N. Tapley, Ed. (Wiley, New York).

Almond, P. R., Wright, A. E. and Boone, M. L. M. (1967). "High-energy electron dose perturbations in regions of tissue heterogeneity Part II: Physical models of tissue heterogeneities," Radiology 88, 1146-1153.

Andreo, P., Hernandez, A., Millan, E. and Millan, S. (1984). "Comments on the transfer of absorbed dose from plastic to water in electron beams," Med. Phys. 11, 874-876.

Asbell, S. O., Siu, J., Lightfoot, D. A. and Brady, L. W. (1980). "Individualized eyeshields for use in electron beam therapy as well as low-energy photon irradiation," Int. J. Radiat. Oncol. Biol. Phys. 6, 519-521.

Berger, M. J. and Seltzer, S. M. (1969). "Calculations of energy and charge deposition and the electron flux in a water medium bombarded with 20 MeV electrons," Ann. N.Y. Acad. Sci. 161, 8-23.

Berkeley, L. W. and Hanson, W. F. (1982). "Measurement of electron beam ionization vs depth of various tissue-like materials," Med. Phys. 9 (abstract), 607.

Biggs, P. J., Boyer, A. L. and Doppke, K. P. (1979). "Electron dosimetry of irregular fields on Clinac-18," Int. J. Radiat. Oncol. Biol. Phys. 5, 433-440.

Boone, M. L. M., Jardine, J. H., Wright, A. E. and Tapley, N. (1967). "High-energy electron dose perturbations in regions of tissue heterogeneity Part I: In vivo dosimetry," Radiology 88, 1136-l145.

Bova, F. (1990). "A film phantom for routine film dosimetry in the clinical environment," Med. Dosimetry 15, 83-85.

Brahme, A. and Svensson, H. (1976). "Specification of electron beam quality from the central-axis depth absorbed-dose distribution," Med. Phys. 3, 95-102.

Brahme, A. (1985). "Current algorithms for computed electron beam dose planning," Radiother. and Oncol. 3, 347-362.

Brahme, A. and Lax, I. (1983). '*Absorbed dose distribution of electron beams in uniform and inhomogeneous media," Acta Radiol. [Suppl.] 364, 61.

Brenner, M., Karjalainen, P., Rytila, A. and Jungar, H. (1969). "The effects of inhomogeneities on dose distribution of high-energy electrons," Ann. N.Y. Acad. Sci. 161, 233-242.

Briot, E. A., Dutreix, J. and Penet, A. J. (1973). "Etude experimental de la collimation des faisceaux d'electrons par un diaphragme de plomb reglable," J. Radiol. Electrol. 54, 39.

Bruinvis, I. A. D. (1985). "Dose calculation for arbitrarily shaped electron beams," p. 210 in *The Computation of Dose Distributions in Electron Beam Radiotherapy,* Nahum, A. E., Ed. (Umea University).

Bruinvis, I. A. D., Heukelom, S. and Mijnheer, B. J. (1985). "Comparison of ionization measurements in water and polystyrene for electron beam dosimetry," Phys. Med. Biol. 30, 1043-1053.

Constantinou, C. (1990). Private communication.

Dahler, A., Baker, A. S. and Laughlin, J. S. (1969). "Comprehensive electron beam treatment planning," Ann. N. Y. Acad. Sci. 161, 198-213.

Deibel, F. C. and Khan, F. M. (1984). Commissioning data (unpublished).

Dixon, R. L. and Ekstrand, K. E. (1986). "Gold and platinum-doped radiation resistant silicon diode detectors," Rad. Prot. Dos. 17, 527-530.

Dutreix, A. and Briot, E. (1985) "The development of a pencil-beam algorithm for clinical use at the Institut Gustave Roussy," p. 242 in *The Computation of Dose Distributions in Electron Beam Radiotherapy,* Nahum, A. E., ed. (Umea University Press).

Dutreix, J. (1970). "Dosimetry", in *Symposium on High-Energy Electrons,* p. 113, Madrid 1966, Gil y Gil and Gil Gayarre, eds. (General Directorate of Health, Madrid).

Dutreix, J. and Dutreix, A. (1969). "Film dosimetry of high energy electrons," Ann. N. Y. Acad. Sci. 161, 33-42.

Ekstrand, K. E. and Dixon, R. L. (1982). "The problem of obliquely incident beams in electron-beam treatment planning," Med. Phys. 9, 276-278.

Ertan, E., Muller-Sievers, K. and Richl, G. (1984). "A new approach to overcome the inconveniences in electron dosimetry associated with the beam scanning technique in linacs," Phys. Med. Biol. 29, 789-796.

Fehrentz, D., Liebig, B. and Schroder-Babo, P. (1976), "Berucksichtigung grosser Inhomogenitatsbereiche bei der Berechnung von Elektronen-Dosisverteilungen," Strahlentherapie, 151, 423.

Fermi, E. (1940). "The ionization loss of energy in gases and condensed materials," Phys. Rev. 57, 485-490.

Gagnon, W. F. and Cundiff, J. H. (1980). "Dose enhancement from backscattered radiation at tissue-metal interfaces irradiated with high-energy electrons," Br. J. Radiol. 53, 466-470.

Galbraith, D. M., Rawlinson, J. A. and Munro, P. (1984). "Dose errors due to charge storage in electron irradiated plastic phantoms," Med. Phys. 11, 197-203.

Gantchew, M. G. and Toush1ekova, .K. (1976). "The influence of the composition of LiF TLD materials on their sensitivity to high energy-electrons," Phys. Med. Biol. 21, 300-308.

Gerbi, B. J. and Khan. F.M. (1987). "The polarity effect for commercially available plane-parallel ionization chambers," Med. Phys., 14, 210-215.

Giarratano, J. C., Duerkes, R. J. and Almond, P. R. (1975). "Lead shielding thickness for dose reduction of 7- to 28-MeV electron," Med. Phys. 2, 336-337.

Goede, M. R. (1985). "Effect of TG21 and ICRU35 polystyreneand plexiglas scaling factors on TG21 electron dosimetry,"677 (abstract WP4-1).

Goede, M. R., Gooden, D. S., Ellis, R. G. and Brickner, T. J. (1977). "A versatile electron collimation system to be used with electron cones supplied with Varian's Clinac-18," Int. J. Radiol. Oncol. Biol. Phys. 2, 791-795,

Hettinger, G. and Svensson, H. (1967). "Photographic film for determination of isodoses from betatron electron radiation," Acta Radiol. 6, 74.

Ho, A. K., Attix, F. H. and Paliwal, B. R. (1985). "Electron solid water for radiotherapy calibration," Med. Phys. 12 (abstract), 677.

Hogstrom, K. R. (1990). Private communication.

Hogstrom, K. R. and Kurup. R. G. (1984). "Derivation of a pencil beam algorithm for arc electron therapy," Med. Phys. 11 (abstract), 361.

Hogstrom, K. R., Mills, M. D. and Almond, P. R. (1981). "Electron beam dose calculation," Phys. Med. Biol. 26, 445-459.

Hogstrom, K. R. (1983). "Dosimetry of electron heterogeneities," p. 223-243 in *Advances in Radiation Therapy Treatment Planning (Medical Physics Monograph No. 9).* Wright, A. E. and Boyer, A. L., Eds. (American Institute of Physics, New York).

Hogstrom, K. R. (1987). "Evaluation ofelectron pencil beam dose calculation," p. *532-561* in *Radiation Oncology Physics-1986 (Medical Physics Monograph No. 15).* Kereiakes, J. G., Elson, H. R. and Born, C. G., Eds. (American Institute of Physics, New York).

Holt, J. G., Mohan, R., Caley, R., Buffa, A., Reid, A., Simpson, L. D. and Laughlin, J. S. (1978). '*Memorial electron beam AET treatment planning system," *70-79* in *Medical Physics Monograph No. 2,* Orton, C. G. and Bagne, F., Eds. (American Institute of Physics, New York).

Horowitz, Y. S. (1984). "Thermoluninescence and Thermoluminescent Dosimetry," Vols. I-III (CRC, Boca Raton).

HPA (1985). Hospital Physicists Association, "Code of practice for electron beam dosimetry in radiotherapy," Phys. Med. Biol. 30, 1169-l194.

ICRU (1972). International Commission on Radiation Units and Measurements, *Radiation Dosimetry: Electrons with Initial Energies Between I and 50 MeV,* ICRU Report 21 (International Commission on Radi-

ation Units and Measurement, Bethesda, Maryland.
ICRU (1978). International Commission on Radiation Units and Measurements, *Dose Specification for Reporting External Beam Therapy with Photons and Electrons*, ICRU Report 29 (International Commission on Radiation Units and Measurement, Bethesda, Maryland).
ICRU (1984). International Commission on Radiation Units and Measurements, *Radiation Dolsimetry: Electron Beams with Energies Between 1 and 50 MeV*, ICRU Report 35 (International Commission on Radiation Units and Measurement, Bethesda, Maryland).
Jamshidi, A., Kuchnir, F. T. and Reft, C. S. (1986). "Determination of the source position for the electron beams from a high-energy linear accelerator," Med. Phys. 13, 942-948.
Khan, F. M., Moore, V. C. and Levitt, S. H. (1976). "Field shaping in electron beam therapy," Br. J. Radiol. 49, 883-886.
Khan, F. M., Sewchand, W. and Levitt, S. H. (1978), "Effect of air space on depth dose in electron beam therapy," Radiology 126, 249-252.
Khan, F. M. and Lee, J. M. F. (1979). 'Computer algorithm for electron beam treatment planning," Med. Phys. 6, 142-144.
Khan, F. M., Werner, B. L. and Deibel, F. C. (1981). "Lead shielding for electrons," Med. Phys. 8, 712-713.
Khan, F. M. (1984). *The Physics of Radiation Therapy*. (Williams and Wilkins, Baltimore, Maryland).
Khan, F. M., Deibel, F. C. and Soleimani-Meigooni, A. (1985). "Obliquity correction for electron beams," Med. Phys. 12, 749-753.
Kirby, T. H., Gastorf, R. J., Hanson, W. F., Berkley, L. W., Gagnon, W. F., Hazle, J. D. and Shalek, R. J. (1985). "Electron beam central axisdepth dose measurements," Med. Phys. 12, 357-361.
Klevenhagen, S. C., Lambert, G. D. and Arbari, A. (1982). "Backscattering in electron beam therapy for energies between 3 and 35 MeV," Phys. Med. Biol. 27, 363-373.
Lambert, G. D. and Klevenhagen, S. C. (1982). "Penetration of backscattered electrons in polystyrene for energies between l-25 MeV," Phys. Med.. Biol. 27, 721-725.
Lanzl, L. H. (1982). "Fundamental interactions of electrons with water," in *Proceedings of the Symposium on Electron Dosimetry and Arc Therapy.* Paliwal, B., Ed. (American Institute of Physics, New York), p. 21-44.
Laughlin, J. S. (1965). "High-energy electron treatment planning for inhomogeneities," Br. J. Radiol. 38, 143.
Laughlin, J. S. and Beattie, J. W. (1951). "Ranges of high energy electrons in water," Phys. Rev. 83, 692-693.
Laughlin, J. S., Lundy, A., Phillips, R., Chu, F. and Sattar, A. (1965). "Electron beam treatment planning in inhomogeneous tissue,"' Radiology 85, 524-531.
Lax, I. and Brahme, A. (1980). "Collimation of high energy electron beams," Acta. Radiol. Oncol. 19, 199-207.
Lax, I., Brahme, A., and Andreo, P. (1983). "Electron beam dose planning using Gaussian beams." Acta Radiol. Suppl. 364, 49.
Loevinger, R., Karzmark, C. J. and Weissbluth, M. (1961). "Radiation therapy with high energy electrons Part 1: Physical considerations 10 to 60 MeV." Radiology 77, 906-927.
Mattsson, L. O., Johansson, K. A. and Svensson, H. (1981). "Calibration and use of plane-parallel ionization chambers for the determination of absorbed dose in electron beams." Acta Radiol. Oncol., 20, 385-399.
McKenzie, A. L. (1979). "Air-gap correction in electron treatment planning," Phys. Med. Biol. 24, 628-635.
Mills, M. D., Hogstrom, K. R., and Fields, R. S. (1985). "Determination of electron beam output factors for a 20 MeV linear accelerator," Med. Phys. 12, 473-476.
Meyer, J. A., Palta, J. R. and Hogstrom, K. R. (1984). "Demonstration of relatively new electron dosimetry measurements techniques on the Mevatron 80," Med. Phys. 11, 670-677.
Mills, M. D., Hogstrom, K. R. and Almond, P. R. (1982). "Prediction of electron beam output factor," Med. Phys. 9, 60-68.
NACP (1981). Supplement to the recommendations by the Nordic Association of Clinical Physics (1980). "Electron beams with mean energies at the phantom surface below 15 MeV," Acta Radiol. Oncol. Rad. Phys. 20, 402-415.
NACP (1980). Recommendations by the Nordic Association of Clinical Physics. "Procedures in external radiation therapy dosimetry with electron and photon beams with maximum energies between 1 and 50 MeV," Acta Radiol. Onc. 19, 55-77.
Nusslin, F. (1974). "Electron back-scattering from lead in a Perspex phantom," (correspondence). Br. J. Radiol. 48, 1041-1042.
Oberhofer, M. and Scharmann, A., Eds. (1981). *Applied Thermoluminescence Dosimetry*, (Adam Hilger, Bristol).
Okumura, Y., Moril, T. and Kitagawa, T. (1971). "Modification of dose distribution in high-energy electron beam treatment," Radiology 99, 683-686.
Okumura, Y. (1972). "Correction of dose distribution for air space in high-energy electron beam therapy," Radiology 103, 183-186.
Parker, R. P., Hobday, P. A. and Cassel, K. J. (1979). "The direct use of CT numbers in radiotherapy dosage calculations for inhomogeneous media," Phys. Med. Biol. 24, 802-809.
Pohlit, W. (1965). Dosimetrie zur Betatrontherapie (Georg Thieme Varlag, Stuttgart).
Pohlit, W. (1969). "Calculated and measured dose distributions in inhomogeneous materials and in patients," Ann. N. Y. Acad. Sci. 161, 189-197.
Prasad, S. C., Bedwinek, J. M. and Gerber, R. L. (1983). "Lung dose in electron beam therapy of chest wall," Acta Radiol. Oncol. 22, 91-95.
Prasad, S. C., Ames, T. E., Howard, T. B., Bassano, D. A., Chung, C. T., King, G. A. and Sagerman, R. H. (1984). "Dose enhancement in bone in electron beam therapy," Radiology 151, 513-516.
Pruitt, J. S. (1987). "Calibration of beta-particle-emitting ophthalmic applicators," Natl. Bur. Stand. (U.S.), Spec. Publ. 250-9 (U.S. Government Printing Office, Washington, D.C.).
Purdy, J. A., Abrath, F. G. and Bello, J. E. (1982). "Electron dosimetry for shaped fields on the Clinac-20," p. 327-338 in *Proceedings of the Symposium on Electron Dasimetry and Arc Therapy,* Paliwal, B., Ed. (American Institute of Physics, New York).
Purdy, J. A., Choi, M. C. and Feldman, A. (1980). "Lipowitz metal shielding thickness for dose reduction of 6-20 MeV electrons," Med. Phys. 7, 251-253.
Rikner, G. and Grusell, E., (1983). "Effects of radiation damage on p-type silicon detectors," Phys. Med. Biol. 28, 1261-1267.
Rikner, G. (1983). "Silicon diodes as detectors in relative dosimetry of photon, electron and proton radiation fields." Ph.D. thesis, Uppsala University.
Rikner, G., (1985). 'Characteristics of a selectively shielded psi detector in ^{60}Co and 8 and 16 MV roentgen radiation," Acta Radiol. Oncol. 24, 205-208.
Rogers, D. W. O. and Bielajew, A. F. (1986). "Differences in electron depth-dosecurves calculated with EGS and ETRAN and improved energy-range relationships," Med. Phys. 13, 687-691.
Rosenblum, L. J., Mauceri, R. A., Wellenstein, D. E., Thomas, F. D., Bassane, D. A., Raasch, B. N., Chamberlain, C. C. and Heitzman, E. R. (1980). "Density patterns in the normal lung as determined by computed tomography," Radiology 137, 409-416.
Saunders, J. E. and Peters V. G. (1974). "Backscattering from metals in superficial therapy with high energy electrons," Br. J. Radiol. 47, 467-470.
Schroder-Babe, P. (1983). "Determination of the virtual electron source of a betatron, Acta Radiol. Suppl. 364, 7-10.
Schultz, R. J. and Meli, J. A. (1984). "Reply to comments of Wu *et al.*," Med. Phys. 11, 872-874.
Schultz, R. J. and Nath, R. (1979). "On the constancy in composition of polystyrene and polymethyl methacrylate plastics," Med. Phys. 6, 153-156.
Sharma, S. C., Deibel, F. C. and Khan, F. M. (1983). "Tissue equivalence of bolus materials for electron beams," Radiology 146, 854-855.
Sharma, S. C., Wilson, D. L. and Jose, B. (1984). "Dosimetry of small fields for Therac 20 electron beams," Med. Phys. 11, 697-702.
Shiragai, A. (1977). "An approach to an analysis of the energy response of LiF-TLD to high-energy electrons," Phys. Med. Biol. 22, 490-499.
Shiu, A. S. and Hogstrom, K. R. (1990). Private communication.
Shortt, K. R., Ross, C. K., Bielajew, A. F., and Rogers, D. W. O. (1986). "Electron beam dose distributions near standard inhomogeneities," Phys. Med. Biol. 31, 235-249.
Sternheimer, R. M. (1952). "The density effect for the ionization loss in various materials, Phys. Rev. 88, 851-859.
Suntharalingam, N. and Cameron, J. R. (1969). "Thermoluminescent response of lithium fluoride to radiations with different LET." Phys. Med. Biol. 14, 397-410.
Suntharalingam, N. and Cameron, J. R. (1969). "Thermoluminescent response of lithium fluoride to high-energy electrons," Ann. N. Y. Acad. Sci. 161, 77-85.
Svensson, H. and Hettinger, G. (1971). "Dosimetric measurements at the nordic medical accelerators Part I. Characteristics of the Radiation Beam," Acta Radiol. Ther. Phys. Biol. 10, 369.
Sze, S. M. (1969). *Physics of Semiconductor Devices*, (Wiley, New York).

Ten Haken, R. K. and Fraass, B. A. (1987). "Relative electron beam measurements: Scaling depths in clear polystyrene to equivalent depths in water," Med. Phys. 14, 410-413.

Ten Haken, R. K., Fraass, B. A., and Jost, R. J. (1987). "Practical methods of electron depth-dose measurement compared to use of the NACP design chamber in water," Med. Phys. 14, 1060-1065.

Thomadsen, B. R., Asp. L. W., Van de Geijn, J., Paliwal, B. R. and Po Cheng, C., (1981). "Perturbation of electron beam doses as a function of SSD due to the use of shielding blocks on the Clinac-18," Med. Phys. 8, 507-509.

Thwaites, D. I. (1985). "Measurements of ionization in water, polystyrene and a 'solid water' phantom material for electron beams," Phys. Med. Biol. 30, 41-53.

van de Geijn, J., Chin, B., Pochobradsky, J. and Miller, R. W. (1987). "A new model for computerized clinical electron beam dosimetry," Med. Phys. 14, 577-583.

Van Dyk, J. Battista, J. J. and Rider, W. D. (1980). "Halfbody radiotherapy: The use ofcomputed tomography to determine the dose to lung," Int. J. Radiat. Oncol. Biol. Phys. 6, 463-470.

Weinhous, M. S. and Meli, J. A. (1984). "Determining P_{ion} the correction factor for recombination losses in an ionization chamber," Med. Phys. 11, 846-849.

Werner, B. L., Khan, F. M. and Deibei, F. C. (1982), "A model for calculating electron beam scattering in treatment planning," Med. Phys. 9, 180-187.

Wong, P. F. (1987). 'Comparison of electron beam depth-dose and off-axis profiles measured with various detectors in water and plastic," M. S. thesis. The University of Texas.

Wu, A., Kalend, A. M., Zicker, R. D. and Sternick, E. S. (1984). "Comments on the method of energy determination for electron beams in the TG-21 protocol," Med. Phys. 11, 871-872.

Zsuia, J., Liuzzi, A. and Laughlin, J. S. (1957). "Oxidation of ferrous sulphate by high-energy electrons and the influence of the polarization effect," Rad. Res. 6, 661-665.

